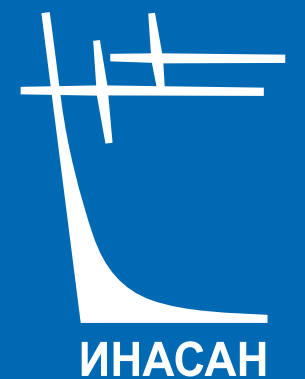


ISSN 2658-5669

НАУЧНЫЕ ТРУДЫ
ИНСТИТУТА
АСТРОНОМИИ РАН

INASAN
SCIENCE
REPORTS

ТОМ
9
ВЫПУСК 2



МОСКВА
2024

В ЖУРНАЛЕ «НАУЧНЫЕ ТРУДЫ ИНСТИТУТА АСТРОНОМИИ РАН» ПУБЛИКУЮТСЯ СТАТЬИ ПО РАЗЛИЧНЫМ АСПЕКТАМ АСТРОНОМИИ, В ТОМ ЧИСЛЕ ПО ТЕОРЕТИЧЕСКОЙ И НАБЛЮДАТЕЛЬНОЙ АСТРОФИЗИКЕ, ПЛАНЕТНОЙ АСТРОНОМИИ, ЗВЕЗДНОЙ АСТРОНОМИИ, ФИЗИКЕ СОЛНЦА, НЕБЕСНОЙ МЕХАНИКЕ АСТРОНОМИЧЕСКИМ МЕТОДАМ И ПРИБОРАМ, КОСМИЧЕСКИМ ИССЛЕДОВАНИЯМ И ИССЛЕДОВАНИЯМ В ОБЛАСТИ КОСМИЧЕСКОЙ ГЕОДЕЗИИ.



УДК 52
ББК 22.6
НЗ4

НЗ4 **Научные труды Института астрономии РАН. Том 9(2).** –
М.: Изд-во Янус-К, 2024, 48 с., илл.

ISSN 2658-5669

e-ISSN 2712-8318

Редколлегия

Сачков М.Е. (главный редактор), Вибе Д.З. (зам. главного редактора),
Бисикало Д.В., Барабанов С.И., Кохирова Г.И., Кузнецов Э.Д., Малков О.Ю.,
Машонкина Л.И., Фатеева А.М., Шематович В.И., Шустов Б.М.

Ответственный редактор Исакова П.Б.

Секретарь редколлегии Вибе Е.Д.

«Научные труды Института астрономии РАН» – рецензируемый журнал, публикующий статьи по различным аспектам астрономии, в том числе по теоретической и наблюдательной астрофизике, планетной астрономии, звездной астрономии, физике Солнца, небесной механике, астрономическим методам и приборам, космическим исследованиям и исследованиям в области космической геодезии.

© ИНАСАН, 2024

© Коллектив авторов, 2024

INASAN Science Reports. Vol 9(2). M.: Janus-K, 2024, 48 pp.

ISSN 2658-5669

e-ISSN 2712-8318

Editorial Board

M.E. Sachkov (Editor-in-Chief), D.S. Wiebe (Deputy Editor-in-Chief),
D.V. Bisikalo, S.I. Barabanov, G.I. Kokhirova, E.D. Kuznetsov, O.Yu. Malkov,
L.I. Mashonkina, A.M. Fateeva, V.I. Shematovich, B.M. Shustov.

Coordinating Editor Isakova P.B.

Staff Editor E.D. Wiebe

INASAN Science Reports is a peer-reviewed journal that publishes papers in various fields of astronomy, including theoretical and observational astrophysics, planetary astronomy, galactic astronomy, solar physics, celestial mechanics, astronomical methods and tools, space research and studies related to space geodesy.

© INASAN, 2024

© Author team, 2024

Учредитель:

Федеральное государственное бюджетное учреждение науки
Института астрономии Российской академии наук

Журнал зарегистрирован в Федеральной службе по надзору
в сфере связи, информационных технологий и массовых коммуникаций
Свидетельство о регистрации ПИ № ФС 77-83927 от 16.09.2022

Научное издание

**Научные труды
Института астрономии РАН.
Том 9 (2)**

Сдано в набор 15.11.2024. Подписано в печать 22.11.2024
Формат 60x90/8. Бумага офсетная.
Уч.-изд. п.л. 6,0. Физ. п.л. 6,0. Тираж 100. Заказ №5264

Издательство «Янус-К»
127411, Москва, Учинская ул., д. 1

Отпечатано в ООО «ИНФОРМ-СОФТ»
119034, Москва, Еропкинский пер., д. 16



Preface

This and the next issues are dedicated to the science results reported at the International Scientific Conference “The BRICS Intelligent Telescope and Data Network”, which was held from 9 to 13 September 2024 in Kazan, Russia.

BRICS is an association of five major emerging economies: Brazil, Russia, India, China, and South Africa. Since December 2023, Egypt, Ethiopia, Iran, and the United Arab Emirates have become members of BRICS, too. The BRICS mechanism aims to promote peace, security, development, and cooperation. It also aims at contributing significantly to the development of humanity and establishing a more equitable and fair world.

Astronomy was established as one of five thematic scientific areas within BRICS at a ministerial meeting held in South Africa in 2014. The goal of BRICS Astronomy Consortium (BAC) is to exploit these basic strengths and common goals for the mutual betterment of our general populaces. The BRICS Astronomy Working Group (BAWG) was then established, with its secretariat based in South Africa. According to official documentation (<https://www.bricsastronomy.org/>) BAWG

- is responsible for promoting cooperation activities in the astronomy priority area;
- convenes BAWG meetings and workshops at least once a year;
- is composed of government officials, focal points (astronomy institutions) and experts;
- is chaired by the South African Department of Higher Education, Science and Technology (DHEST) which provides secretariat support.

The BRICS Astronomy Consortium has laid a good foundation and made progress over the years, evident in that finally in 2021 the consortium was successfully granted seed funding to work on the flagship project “The BRICS Intelligent Telescope and Data Network (BITDN) Project”. The flagship programme is based on a merger of the two leading proposals: astronomy transients and big data which were presented, discussed and voted at the annual BAWG meetings in 2018 and 2019. The combined programme is currently ongoing and involves astrophysical transients, survey science and time domain astronomy. It has plans to involve forefront observational facilities and the big data/computational infrastructure needed to support them. Existing and new facilities in all BRICS countries and others where there is access, will be harnessed and developed to support the programme.

According to the BRICS STI Calendar of Activities for 2023–2024 adopted at the 11th BRICS STI Ministerial Meeting (Qheberha, South Africa, 4 August 2023) Russia has hosted the 10th Meeting of the BRICS Astronomy Working Group Meeting (BAWG). The Meeting as well as the International Scientific Conference “The BRICS Intelligent Telescope and Data Network” has been held in marvelous city. The Meeting and the Conference were organized by the Ministry of Science and Higher Education of the Russian Federation with the support of the Kazan Federal University¹.

Scientists from Russia, Brazil, India, China, South Africa, Iran, and Kazakhstan took part in the conference. 55 talks were presented, most of which were in person. The most interesting papers, based on the talks, were selected by the Scientific Committee for publication in this issue.

On behalf of the Program Committee

A. Pozanenko
E. Kuznetsov
B. Shustov
D. Buckley

¹<https://kpfu.ru/eng/academic-units/physics-mathematics-and-it/institute-of-physics/structure/departments/department-of-astronomy-and-cosmic-geodesy/engelgardt-astronomical-observatory/brics-astronomy-2024/general-information>



Participants of the Meeting and the Conference during a visit to the Engelhardt Observatory and Planetarium of Kazan University.

Восстановление коронального магнитного поля при помощи ограниченной оптимизации по данным SDO/HMI

Джафарпур М.Х., Фатхолазаде С., Насири С.

Физический факультет, Университет им. Шахида Бехешти, 1983969411, Тегеран, Иран

Хорошо известно, что динамика солнечной короны определяется магнитным полем. С другой стороны, измерить величину и определить структуру коронального магнитного поля невозможно из-за теплового уширения. По этой причине поле в короне может быть реконструировано с использованием данных, полученных с помощью магнитограммы и физики бессильных полей. Здесь мы предлагаем метод ограниченной оптимизации с использованием векторного множителя Лагранжа и сравниваем результаты с результатами существующих моделей. Численный анализ нашей модели был проведен с помощью наблюдательной векторной магнитограммы, полученной с помощью изображений SDO/HMI. Мы приходим к выводу, что 1) лагранжиан в настоящей модели сходится немного быстрее, чем в моделях сравнения. 2) Поведение магнитной свободной энергии в процессе оптимизации согласуется с поведением в предыдущих исследованиях. 3) Разработана модель для реальной магнитограммы. Вычислены такие величины, как содержание магнитной энергии, текущий взвешенный угол между вектором плотности тока и магнитным полем и относительные ошибки потока.

Поступила в редакцию 28.09.2024 г. Принята в печать 13.10.2024 г.

Ключевые слова: солнечная корона, солнечные магнитные поля, солнечная активность, солнечные вспышки, анализ данных

Reconstruction of coronal magnetic field by constraint optimization using the SDO/HMI data

Jafarpour M.H., Fatholahzadeh S., Nasiri S.

Department of Physics, Shahid Beheshti University, 1983969411, Tehran, Iran

It is well known that the dynamics of the solar corona is governed by the magnetic field. On the other hand due to the thermal broadening it is not possible to measure the magnitude and determine the structure of the coronal magnetic field. For this reason, the field in the corona may be reconstructed using the data obtained by the magnetogram and the physics of force-free fields. Here we propose a method of constrained optimization using the vector Lagrange multiplier and compare the results with those of ever present models. The numerical analysis of the our model was conducted through an observational vector magnetogram obtained by *SDO/HMI* images. We conclude that i) the Lagrangian in the present model converges slightly faster than that of comparison models. ii) the behavior of the magnetic free energy during the optimization is compatible with those of the previous studies, iii) the model is worked out for a real magnetogram and the corresponding quantities such as magnetic energy content, the current weighted angle between the current density vector and magnetic field, and the fractional flux errors are computed.

Received 28.09.2024. Accepted 13.10.2024.

Keywords: Solar corona, Solar magnetic fields, Solar activity, Solar flares, data analysis

DOI: 10.51194/INASAN.2024.9.2.001

1. Introduction

The solar coronal structures are mainly formed and evolved in accordance with the coronal magnetic field and one can ignore other forces such as pressure gradient, gravitational, and dissipative forces in studying the dynamics of these structures. While the Lorentz force is important, however, determination of the magnetic field in the solar corona is currently impossible due to the fact that thermal broadening of the Zeeman lines swamps the magnetic broadening [1].

One way to overcome the problem and to find the magnetic field in the solar corona is to reconstruct it through extrapolation of magnetogram data [2, 3]. Since the coronal structures are in equilibrium under a single Lorentz force, the corresponding magnetic field must be force-free. Several models have been developed following the rules of force-free magnetic fields. Thus, it is expected that the Lorentz force should vanish for the solar coronal magnetic field, $\mathbf{B} \equiv \mathbf{B}(x, y, z)$,

$$(\nabla \times \mathbf{B}) \times \mathbf{B} = 0, \quad (1)$$

where x, y, z denotes the space coordinates. In addition the physical magnetic field must be solenoidal

$$\nabla \cdot \mathbf{B} = 0. \quad (2)$$

A solution for the above equations is

$$\nabla \times \mathbf{B} = \alpha(r)\mathbf{B}, \quad (3)$$

where $\alpha(r)$ is in general is a scalar function of spatial coordinates, which is zero for potential fields, constant for linear force-free fields, and a scalar function of the spatial coordinates for non-linear force-free magnetic fields.

Since a general solution does not exist for Eqs. (1) and (2), authors of [4] obtained a semi-analytical solution for these equations (hereafter L&L). A comprehensive review of the models of reconstruction of force-free magnetic fields can be found in [5]. Among these models, the optimization model developed in [6] has received more attention (hereafter referred to as WSR). However, the WSR model has been frequently revised. For instance, authors of [7] modified this model by considering a Weighting Function (hereafter denoted as OWF) and by adding a layer to the top and lateral sides boundaries. [3] added an integral term to the Lagrangian containing the measurement errors of SDO/HMI magnetogram and used a constant Lagrange multiplier to account for the injection speed of the boundary conditions and measurement errors.

The WSR optimization model is now more popular due to faster computations, ease of understanding, and cost-effectiveness. As another approach to the optimization model, authors of [8] employed the Lagrange multiplier technique to develop a constrained optimization model that may be referred to as Constrained Optimization by Scalar Lagrange multiplier function (COS). In section 2, the theoretical approach is introduced. In section 3 the numerical analysis is given. Finally, in section 4 the model is applied to a real vector magnetogram including the AR 11543. Section 5 is devoted to concluding remarks.

2. Theoretical approach

In the WSR model as well as the similar optimization methods, an appropriate Lagrangian is employed to reconstruct a convenient magnetic field in the solar corona. In the COV model (Constrained Optimization with the Vector Lagrange multiplier), as an extension of the COS approach, we use the optimization principle by employing a vector Lagrange multiplier. This is done by considering Eq. (2) as the governing equation of solenoidal nature and Eq. (1) as the constraint fixing the force-freeness nature of the magnetic field. Then by minimizing the term $|\nabla \cdot \mathbf{B}|$ subject to the constraint $(\nabla \times \mathbf{B}) \times \mathbf{B} = 0$ using Lagrange multiplier technique, an appropriate Lagrangian is proposed as

$$L_{\text{COV}} = L_d + L_f = \int_v \omega_d |\nabla \cdot \mathbf{B}|^2 dv + \int_v \omega_f (\boldsymbol{\lambda} \cdot [(\nabla \times \mathbf{B}) \times \mathbf{B}]) dv, \quad (4)$$

where ω_d and ω_f are weighting functions, and indices d and f refer to divergence-free and force-free functions, respectively. In the same manner as COS model, $\mathbf{B} \equiv \mathbf{B}(x, y, z, t)$ and $\boldsymbol{\lambda} \equiv \boldsymbol{\lambda}(x, y, z, t)$ denote the magnetic field and the vector Lagrange multiplier, respectively. Using the Lagrange multiplier as a vector field is due to the vector behavior of the constraint equation in Lagrangian of Eq. (4). In the same manner the scalar nature of the Lagrange multiplier in COS model was due to the scalar behavior of the corresponding constraint equation ($\nabla \cdot \mathbf{B} = 0$). As a result, to have scalar Lagrangian, both terms in Eq. (4) become scalar quantities. Taking the derivative of Eq. (4) and by some appropriate vector algebra, one gets

$$\begin{aligned} \frac{\partial L_{\text{COV}}}{\partial t} &= \int_v [(\frac{\partial \mathbf{B}}{\partial t} \cdot \mathbf{F}_{\text{COV}}(\mathbf{B}, \boldsymbol{\lambda})) + (\frac{\partial \boldsymbol{\lambda}}{\partial t} \cdot \mathbf{H}_{\text{COV}}(\mathbf{B}, \boldsymbol{\lambda}))] dv \\ &+ \int_s (\frac{\partial \mathbf{B}}{\partial t} \cdot \mathbf{G}_{\text{COV}}(\mathbf{B}, \boldsymbol{\lambda})) ds, \end{aligned} \quad (5)$$

where

$$\mathbf{F}_{\text{COV}}(\mathbf{B}, \boldsymbol{\lambda}) = \omega_f (\boldsymbol{\lambda} \times (\nabla \times \mathbf{B})) + \omega_f (\nabla \times (\mathbf{B} \times \boldsymbol{\lambda})) \quad (6)$$

$$+ \nabla \omega_f \times (\mathbf{B} \times \boldsymbol{\lambda}) - 2[(\nabla \cdot \mathbf{B}) \nabla \omega_d + \omega_d \nabla (\nabla \cdot \mathbf{B})],$$

$$\mathbf{G}_{\text{COV}}(\mathbf{B}, \boldsymbol{\lambda}) = 2\omega_d (\nabla \cdot \mathbf{B}) \mathbf{n} + (\mathbf{B} \times \boldsymbol{\lambda}) \times \omega_f \mathbf{n}, \quad (7)$$

and

$$\mathbf{H}_{\text{COV}}(\mathbf{B}, \boldsymbol{\lambda}) = \omega_f [(\nabla \times \mathbf{B}) \times \mathbf{B}]. \quad (8)$$

For details of calculations see [9]. To reconstruct the field over an active region, we assume a box whose lower side coincides with the given magnetogram, while the lateral and top sides are in the solar corona and satisfies appropriate boundary conditions.

We reconstruct the magnetic field inside the computational box by extrapolation of the photospheric magnetic field in the given magnetogram. Assuming that no active region is located near the edges of the magnetogram,

we expect that the magnetic field of the lateral boundaries of the box would remain unchanged throughout the iteration procedure; that is

$$\left(\frac{\partial \mathbf{B}}{\partial t}\right)_s = 0. \quad (9)$$

Thus, the surface integral in Eq. (5) vanishes and the volume integrals in Eq. (5) will always be negative assuming

$$\frac{\partial \lambda}{\partial t} = -\mu_1 \mathbf{H}_{\text{COV}}(\mathbf{B}, \lambda), \quad (10)$$

and

$$\frac{\partial \mathbf{B}}{\partial t} = -\mu_2 \mathbf{F}_{\text{COV}}(\mathbf{B}, \lambda), \quad (11)$$

where μ_1 and μ_2 are positive parameters to be specified during numeric calculations. Note that, μ_1 and μ_2 have the dimensions of $\frac{1}{B^2}$ and l^2 , respectively. Using Eqs. (10) and (11) in Eq. (5) one may obtain

$$\frac{1}{2} \frac{\partial L_{\text{COV}}}{\partial t} = - \int_v (\mu_1 |\mathbf{H}_{\text{COV}}(\mathbf{B}, \lambda)|^2 + \mu_2 |\mathbf{F}_{\text{COV}}(\mathbf{B}, \lambda)|^2) dv. \quad (12)$$

Thanks to the minimization mechanism inherent in Eq. (12) one may choose an arbitrary λ , and \mathbf{B} as an initial input, and follow their evolution through the coupled Eqs. (10), and (11). Since the final task is to find the magnetic field satisfying the appropriate boundary conditions, one may use a potential magnetic field (\mathbf{B}_0) as the input field, and a suitable ansatz for the initial value of the λ in terms of \mathbf{B}_0 as follows

$$\lambda \equiv \lambda_0 = |\mathbf{B}_0|^{-2} [(\nabla \times \mathbf{B}_0) \times \mathbf{B}_0]. \quad (13)$$

Finally choosing a positive L_{COV} at the beginning, it will approach zero at the end of the iteration. The Lagrange multiplier, λ , and magnetic field, \mathbf{B} , are updated simultaneously at each iteration step according to Eqs. (10) and (11), respectively. Thus, following the optimization procedure, one may reconstruct the expected divergence-free and force-free output magnetic field by the COV model to the extent that the boundary conditions are consistent.

3. Numerical analysis

It is well understood that non-linear force-free reconstruction models do not relax to an exactly force-free state, even using the weighting function approach of the [7] to reduce the boundary mismatches [10].

This is due to the different factors such as lack of top and lateral sides boundary data, inconsistency of the boundary condition of \mathbf{B}_z (or α) with a nonlinear force-free magnetic field, the errors and noises in the magnetogram measurements, deviations of the photospheric magnetic field from the nonlinear force-free magnetic field, etc. [11, 10]. The convergency considered here is reliable insofar as the above problems are fulfilled. Nevertheless, one must try to find a maximal consistency of force-free magnetic field with the given boundary data. Preprocessing of the measured vector magnetogram data is in this respect, which we will apply to the real magnetogram.

3.1. Applying the model to a real vector magnetogram

The COV model is applied to a vector magnetogram image of SDO/HMI, which provides a vector magnetic field with high spatial and temporal resolution [12]. One may follow preprocessing operation using the Aly criteria [13].

The magnetogram includes the active region AR 11543 and has been observed at 00 : 12 UT, 13 August, 2012 and has 640×640 pixels with a spatial resolution of $\simeq 370$ km per pixel. The target area has been selected in such a way that the active region are located far enough from its boundaries. The computational box is considered to have 80 pixel along the z axis and the thickness of the boundary layer is assumed as $n_d = 4$.

We assume the standard data set for the preprocessing parameters, $\mu_1 = 1$, $\mu_2 = 1$, $\mu_3 = 0.001$, $\mu_4 = 0.01$, as given by [1] notation to correct the force-freeness, the torque-freeness, the optimized boundary matches with the photospheric data, and the smoothing, respectively.

Optimizing the real magnetogram, the Lagrangian reaches 0.004 of its initial value after 4000 iteration steps. The iterative behaviour of Lagrangian L is shown in Fig. (1). In addition, the average value of the fractional flux errors, $\langle |f_i| \rangle$ was reached to 1.33×10^{-3} for physical box as shown in Fig. (2), indicating that the final state, when using real magnetogram, is almost close to divergence-free solution all over the grid points.

Furthermore, the current weighted angle between the current density vector and magnetic field, θ_J , reduces from 59.06° and 56.69° at the beginning to 13.11° and 10.61° at the end of iteration for computational and physical box, respectively. The ratio of magnetic energy to the potential one is calculated to be 1.185 in the box as shown in Fig. (3). Thus, the free magnetic energy content, $E_{\text{free}} = E_F - E_P$, inside the box is estimated to be 2.20×10^{29}

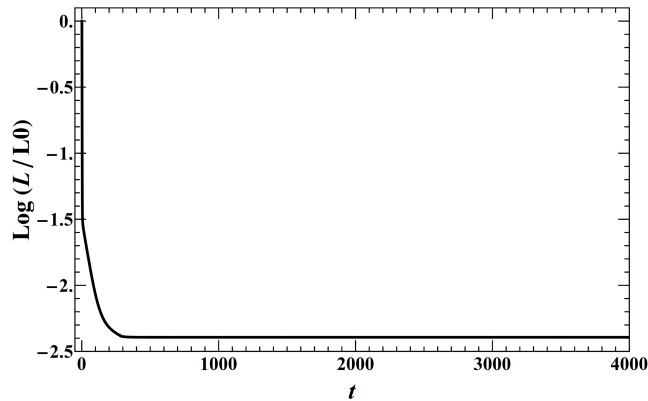


Figure 1: The behavior of the normalized Lagrangian, $\frac{L(\mathbf{B}, \lambda)}{L_0(\mathbf{B}, \lambda)}$, in logarithmic scale using COV model.

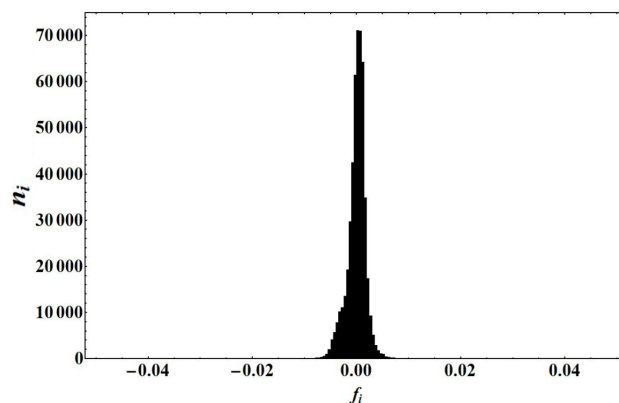


Figure 2: Distribution of fractional flux errors, $\langle |f_i| \rangle$ over all grid points for the COV model.

erg. One may refer to the flaring behaviour of this active region at Heliophysics Event Catalogue¹. Some of the closed reconstructed nlfff lines are plotted over the given magnetogram in Fig. 4.

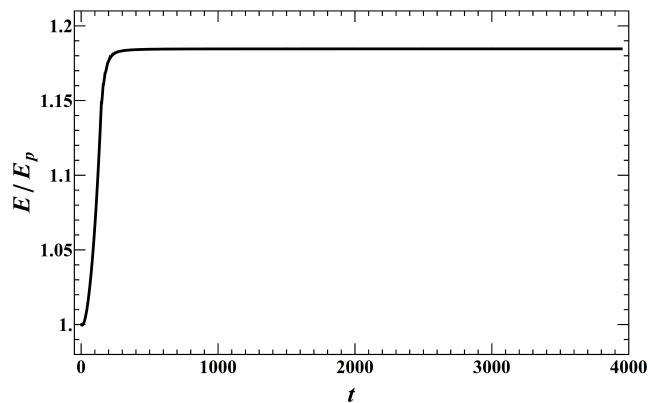


Figure 3: The behavior of the ratio of the reconstructed to the potential magnetic energies during the iteration for the real magnetogram.

4. Conclusions

According to the coronal conditions the effect of non-magnetic forces on the dynamical behavior of the corona, such as pressure gradient, and gravity forces can be ignored. Due to technical problems, direct measurement

¹http://helio.mssl.ucl.ac.uk/helio-vo/solar_activity/arstats/arstats_page5.php?region=11543

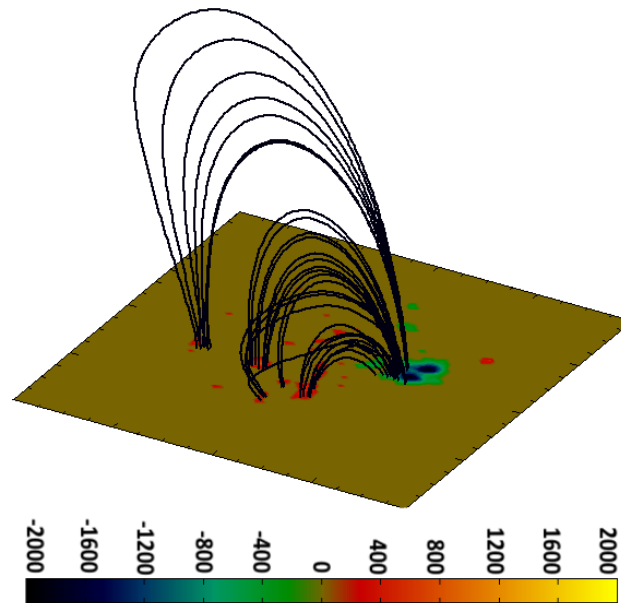


Figure 4: The nlff lines for the magnetogram of AR 11543. The color bar shows the strength (in Gauss) and polarity of the magnetic field.

of the magnetic field in the solar corona is impossible. Therefore, one may reconstruct the magnetic field using photospheric data obtained by the magnetograms.

As a constrained optimization technique, we used a vector Lagrange multiplier technique, COV model, to reconstruct a force-free magnetic field. The magnetic field is reconstructed inside a computational box over a given real magnetogram. The initial potential magnetic field is obtained as a solution of the Laplace equation using Green's function method [14], and the reconstruction is implemented by optimizing a Lagrangian constructed by a solenoidal field subject to the constrained equation governing a force-free magnetic field. As an advantage of COV model, the Lagrangian and the angle between electric current density and magnetic field approaches zero faster than that of comparison models at least for initial iteration steps. This behavior may be helpful when one deals with time series events, while several magnetograms must be considered and limited steps of iteration are needed.

References

1. T. Wiegelmann, B. Inhester, and T. Sakurai, *Sol. Phys.*, **233**, 215, 2006.
2. J. Schou, J. M. Borrero, A. A. Norton, S. Tomczyk, D. Elmore, and G. L. Card, *Sol. Phys.*, **275**, 327, 2012.
3. T. Wiegelmann, J. K. Thalmann, B. Inhester, T. Tadesse, X. Sun, and J. T. Hoeksema, *Sol. Phys.*, **281**, 37, 2012.
4. B. C. Low and Y. Q. Lou, *APJ*, **352**, 343, 1990.
5. T. Wiegelmann and T. Sakurai, *Living Reviews in Solar Physics*, **18**, 1, 2021.
6. M. S. Wheatland, P. A. Sturrock, and G. Roumeliotis, *APJ*, **540**, 1150, 2000.
7. T. Wiegelmann, *Sol. Phys.*, **219**, 87, 2004.
8. S. Nasiri and T. Wiegelmann, *JASTP*, **182**, 181, 2019.
9. S. Fatholahzadeh, M. H. Jafarpour, and S. Nasiri, *A&A*, **676**, A120, 2023.
10. M. L. De Rosa, C. J. Schrijver, G. Barnes, K. D. Leka, et al., *APJ*, **696**, 1780, 2009.
11. M. L. DeRosa, M. S. Wheatland, K. D. Leka, G. Barnes, et al., *APJ*, **811**, 107, 2015.
12. J. Schou, P. H. Scherrer, R. I. Bush, R. Wachter, et al., *Sol. Phys.*, **275**, 229, 2012.
13. J. J. Aly, *Sol. Phys.*, **120**, 19, 1989.
14. N. Seehafer, *Sol. Phys.*, **58**, 215, 1978.

Аккреционные вспышки в массивных молодых звездных объектах

Зинченко И.И.

Федеральный исследовательский центр Институт прикладной физики им. А.В. Гапонова-Грехова Российской академии наук, Нижний Новгород, Россия

Вспышки светимости в маломассивных (прото)звездах, обычно объясняемые эпизодической аккрецией, известны уже несколько десятилетий. Недавно подобные события были обнаружены в массивных молодых звездных объектах (МЗО). Существуют теоретические модели, предсказывающие такое поведение. Одна из первых таких вспышек была зарегистрирована в направлении МЗО S255IR NIRS3 с массой $20 M_{\odot}$, который мы долгое время изучали на разных масштабах с помощью нескольких инструментов. Здесь мы представляем краткий обзор наших исследований этого объекта, а также исследований подобных вспышек в других массивных МЗО. В целом это явление подтверждает сценарий эпизодической дисковой аккреции как механизма формирования звезд с массами до $\sim 20 M_{\odot}$.

Поступила в редакцию 04.10.2024 г. Принята в печать 14.11.2024 г.

Ключевые слова: образование звезд, массивные звезды, аккреционные вспышки

Accretion outbursts in massive young stellar objects

Zinchenko I.I.

Federal Research Center A.V. Gaponov-Grekhov Institute of Applied Physics of the Russian Academy of Sciences, Nizhny Novgorod, Russia

Luminosity outbursts in low-mass (proto)stars, explained usually by episodic accretion, have been known for decades. Recently, similar events have been detected in massive young stellar objects (YSO). There are theoretical models which predict such a behavior. One of the first such outbursts was registered towards the $20 M_{\odot}$ YSO S255IR NIRS3, which we have been investigating for a long time at various scales with several instruments. Here we present a brief review of our studies of this object and studies of similar outbursts in other massive YSOs. In general, this phenomenon supports the scenario of episodic disk accretion as a formation mechanism for stars with masses up to $\sim 20 M_{\odot}$.

Received 04.10.2024. Accepted 14.11.2024.

Keywords: star formation, massive stars, accretion outbursts

DOI: 10.51194/INASAN.2024.9.2.002

1. Introduction

The process of high mass star formation is still poorly understood (e.g., [1, 2, 3, 4]). A key question is whether this process is a scaled-up version of the low-mass star formation or is significantly different. Observations at various scales and regular monitoring in various bands are essential for selection between different scenarios. Observational studies are complicated by the rarity of massive (proto)stars and, accordingly, large distances to them.

The accretion flow can be irregular due to disk fragmentation. Such a behavior in low-mass (proto)stars is confirmed by luminosity outbursts, which have been observed in these objects for decades (FUor and EXor outbursts). There are theoretical models which predict similar behavior in high-mass star formation (e.g., [5, 6]). In recent years several such events have been detected in high-mass young stellar objects (YSO) [7]. One of the first of them was registered towards the $20 M_{\odot}$ YSO S255IR NIRS3 as an IR and methanol maser flares [8, 9, 10]. This object belongs to the well-known star-forming complex sandwiched between the evolved H II regions S255 and S257 [11]. We have investigated this area at various scales [12] with several single-dish radio telescopes (IRAM-30m, OSO-29m, MPIfR 100-m) and with radio interferometers (ALMA, GMRT, SMA, VLA). Here we present a brief review of our studies of this object and studies of similar outbursts in other massive YSOs.

2. Outbursts in S255IR NIRS3

Our investigations of the S255IR area include imaging in continuum and in many molecular lines. The frequency coverage was from ~ 600 MHz (GMRT) to ~ 350 GHz (ALMA). The angular resolution achieves ~ 15 milliarcseconds (for ALMA observations), which corresponds to ~ 25 au at the distance to S255 ($1.78^{+0.12}_{-0.11}$ kpc from the maser parallax measurements [13]). In addition, we combine our radio data with our and other available data in other bands. In our ALMA observations we detected a burst in the submillimeter continuum [14] and a new, never predicted methanol maser line [15].

In Figure 1 (left panel) we present a composite image of the central part of the S255IR clump in the NIR $2.12 \mu\text{m}$ H₂ and $1.64 \mu\text{m}$ Fe II lines [16], and in the 0.9 mm ALMA continuum emission [17]. The high velocity HCN(4–3) emission [18] is also shown.

These NIR lines are shock tracers and two knots, bright in these lines, are associated apparently with bow shocks produced by the jet. They have non-thermal radio spectra [19] indicating the presence of relativistic

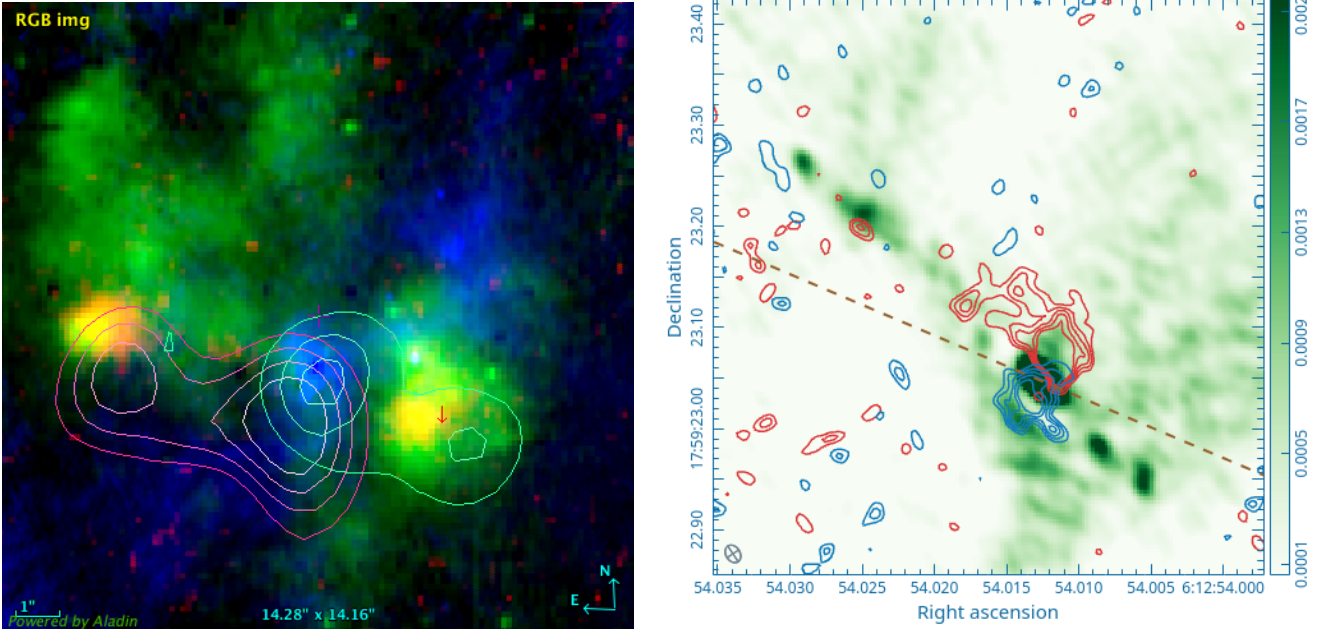


Figure 1: Left panel: S255IR area in the $2.12 \mu\text{m}$ H_2 line (green), $1.64 \mu\text{m}$ Fe II (red) and 0.9 mm ALMA continuum emission (blue). The magenta and cyan contours show the high-velocity HCN(4–3) emission. The NIR data are from SINFONI observations [16]. The radio data are from [18, 17]. Right panel: the image of S255IR area in continuum obtained with ALMA at 0.9 mm with $\sim 15 \text{ mas}$ resolution (Zinchenko, Liu & Su, submitted). The knots in the jet are marked. The red and blue contours show the emission in the $\text{C}^{34}\text{S}(7-6)$ line wings. The dashed line indicates the jet orientation at larger scales ($\text{PA} = 67^\circ$).

electrons and magnetic field. Their minimum energy and minimum magnetic field strengths, calculated from the equipartition theorem are 4.5×10^{41} ergs and 1.1 mG respectively [19]. With the projected velocity of $\sim 450 \text{ km s}^{-1}$ for the NE lobe [20, 21] and $\sim 285 \text{ km s}^{-1}$ for the SW lobe [22] the ejection of these knots happened about 60–70 years ago [12]. The HCN(4–3) emission (Figure 1) as well as the $\text{HCO}^+(4-3)$ emission observed here, too [18], imply the presence of dense high-velocity molecular gas, probably entrained by the bow shock.

There are more H_2 knots, approximately in the same direction at quasi-regular intervals [12]. They imply several ejection events during last centuries. The direction of these ejections coincides with the orientation of the IR jet (the position angle $\text{PA} = 67^\circ$) discovered in this area many years ago [23].

In 2015 an outburst at NIR wavelengths [8] and 6.7 GHz methanol maser flare [24] were recorded. The configuration of the maser spots in the source changed significantly [9]. A comparison of our observations of this object with ALMA in 2016–2017 with our observations with the SMA in 2010 shows a burst at the wavelength of 0.9 mm [14]. At the same time we detected a new, never predicted methanol maser line in the $14_1 - 14_0 \text{ A}^{++}$ transition at 349.1 GHz . In 2017 both the 0.9 mm continuum and this maser line were weaker than in 2016, indicating a decay of the burst.

The main results obtained in that period can be summarized as follows. Bolometric luminosity of S255IR NIRS3 increased by about a factor of 5.5, from $3 \times 10^4 L_\odot$ to $1.6 \times 10^5 L_\odot$ [8]. Energy release was $(1.2 \pm 0.4) \times 10^{46}$ erg, which corresponds to accretion of about 2 Jupiter masses. According to the submillimeter data [14], dust temperature increased by a factor of 2, which implies an increase in luminosity by a factor of 16. The difference can be due to the difference in beam sizes. In IR observations it was much larger ($\sim 6''$) than in our submillimeter observations and covered neighboring objects. The burst duration was about 2 years. The accretion rate during the burst achieved $\sim 5 \times 10^{-3} M_\odot/\text{year}$. An analysis of the $14_1 - 14_0 \text{ A}^{++}$ methanol maser excitation shows that lines of this series can be tracers of such outbursts [25].

In 2021 new ALMA observations of this object were carried out with the angular resolution of ~ 15 milliarcseconds, which is almost an order of magnitude higher than in the previous studies [26]. In Figure 1 (right panel) we present the image of the S255IR area in continuum overlaid with contours of the emission in the $\text{C}^{34}\text{S}(7-6)$ line wings obtained in these observations.

The data show a bright central source (the brightness temperature is $\sim 850 \text{ K}$) and two pairs of bright knots in the jet, one pair in each jet lobe. The distances between the knots in the pairs correspond to the time interval of about 1.5 years, taking into account the lobe velocities mentioned above. Probably this implies a double ejection. The light curve of the 6.7 GHz methanol maser at the velocity of 2.87 km s^{-1} has two peaks with the same time interval between them [10].

The orientation of the jet differs by $\sim 20^\circ$ from that on larger scales, as mentioned also in some other recent works [21, 27]. This implies a strong jet precession.

A comparison with the observations at lower frequencies [19, 21] shows that the emission of the central source is a mixture of the dust emission and free-free emission of the ionized gas. The estimates of the emission measure and electron density are rather typical for hypercompact H II regions [26]. In the emission of the knots in the jet a free-free component apparently dominates.

An analysis of the position-velocity diagrams in various lines shows that the disk rotation is sub-Keplerian. At the same time we see a deep absorption in molecular lines towards the central bright source. The deepest absorption features are red-shifted relative the core velocity, which may indicate an infall.

The emission in continuum and in molecular lines looks very inhomogeneous as can be seen in Figure 1. However, regular patterns are present in the continuum map, which can be a result of interferometric filtering and/or data processing. At the same time, the inhomogeneity in the molecular maps is most probably real. Apparently, it reflects a small-scale clumpiness in the source. However, no large-scale coherent structures, expected in some models, are observed.

The methanol maser emission in the $14_1 - 14_0$ A^{-+} transition still persists although its integrated flux is much lower than in 2016. A maser emission with about the same intensity was observed in the $12_1 - 12_0$ A^{-+} transition, too [12]. The peak of this maser emission is located towards the red-shifted lobe of the jet. One more Class II methanol maser line ($6_1 - 5_2$ E) was detected in the same area [28].

3. Outbursts in other massive young stellar objects

To date, similar events have been recorded in 6 objects [7]. Masses of these objects range from $\sim 5 M_\odot$ to $\sim 23 M_\odot$, the luminosity increases by a factor of $\sim 5 - 16$, the burst duration is from ~ 1 year to ~ 10 years, the energy release reaches $\sim 10^{47}$ erg, the accreted mass is estimated to be from ~ 1 to ~ 7 Jupiter masses.

The luminosity outbursts are observed at various wavelengths and in most cases they are accompanied by Class II methanol maser flares (mostly in the 6.7 GHz transition but also some other maser transitions can be excited).

In general, this phenomenon supports the scenario of episodic disk accretion as a formation mechanism for stars with masses up to $\sim 20 M_\odot$.

4. Summary and conclusions

In this review we briefly described recent investigations of the accretion outbursts in massive YSOs with an emphasis on the $\sim 20 M_\odot$ S255IR NIRS3 protostar, which has been a target of our long-term studies. The main points can be summarized as follows:

1. Observations at scales of $\sim 1'$ indicate quasi-regular ejections in approximately the same direction from S255IR-SMA1 (NIRS3, mass $\sim 20 M_\odot$) over the past ~ 1000 years.
2. The orientation of the last ejection (happened in 2015) differs by $\sim 20^\circ$ (in projection). The ejection was double with an interval of ~ 1.5 years.
3. There is an ionized region with characteristics of a hypercompact H II region around NIRS3, as well as a dust shell.
4. Submillimeter emission from knots in the jet is probably mainly bremsstrahlung from ionized gas.
5. A highly inhomogeneous quasi-Keplerian disk with signs of infall motions is observed.
6. There is a maser emission in the CH_3OH 12_1-12_0 and 14_1-14_0 A^{-+} lines, with the emission peak towards the red-shifted lobe of the jet. The Class II maser emission in other CH_3OH lines is observed in this area, too. These maser lines can probably serve as tracers of such outbursts.
7. To date, accretion bursts have been recorded in several massive YSOs with masses from $\sim 5 M_\odot$ to $\sim 23 M_\odot$. The burst duration is from ~ 1 year to ~ 10 years, the energy release reaches $\sim 10^{47}$ erg, the accreted mass is estimated to be from ~ 1 to ~ 7 Jupiter masses.
8. Overall, the observed outbursts in massive YSOs support the scenario of episodic disk accretion as a formation mechanism for stars with masses up to $\sim 20 M_\odot$.

Funding

This work was supported by the Russian Science Foundation grant number 24-12-00153 (<https://rscf.ru/en/project/24-12-00153/>).

References

1. J. C. Tan, M. T. Beltrán, P. Caselli, F. Fontani, A. Fuente, M. R. Krumholz, C. F. McKee, and A. Stolte, *Protostars and Planets VI*, 149–172, 2014.
2. F. Motte, S. Bontemps, and F. Louvet, *ARA&A*, **56**, 41, 2018.

3. A. L. Rosen, S. S. R. Offner, S. I. Sadavoy, A. Bhandare, E. Vázquez-Semadeni, and A. Ginsburg, *Space Sci. Rev.*, **216**, 62, 2020.
4. P. Padoan, L. Pan, M. Juvela, T. Haugbølle, and Å. Nordlund, *ApJ*, **900**, 82, 2020.
5. D. M.-A. Meyer, E. I. Vorobyov, R. Kuiper, and W. Kley, *MNRAS*, **464**, L90, 2017.
6. D. M. A. Meyer, E. I. Vorobyov, V. G. Elbakyan, B. Stecklum, J. Eislöffel, and A. M. Sobolev, *MNRAS*, **482**, 5459, 2019.
7. V. Wolf, B. Stecklum, A. Caratti o Garatti, P. A. Boley, et al., *A&A*, **688**, A8, 2024.
8. A. Caratti O Garatti, B. Stecklum, R. Garcia Lopez, J. Eislöffel, et al., *Nature Physics*, **13**, 276, 2017.
9. L. Moscadelli, A. Sanna, C. Goddi, M. C. Walmsley, et al., *A&A*, **600**, L8, 2017.
10. M. Szymczak, M. Olech, P. Wolak, E. Gérard, and A. Bartkiewicz, *A&A*, **617**, A80, 2018.
11. D. K. Ojha, M. R. Samal, A. K. Pandey, B. C. Bhatt, et al., *ApJ*, **738**, 156, 2011.
12. I. I. Zinchenko, S. Y. Liu, D. K. Ojha, Y. N. Su, and P. M. Zemlyanukha, *arXiv e-prints*, arXiv:2408.03133, 2024.
13. R. A. Burns, T. Handa, T. Nagayama, K. Sunada, and T. Omodaka, *MNRAS*, **460**, 283, 2016.
14. S.-Y. Liu, Y.-N. Su, I. Zinchenko, K.-S. Wang, and Y. Wang, *ApJ*, **863**, L12, 2018.
15. I. Zinchenko, S.-Y. Liu, Y.-N. Su, and A. M. Sobolev, *A&A*, **606**, L6, 2017.
16. Y. Wang, H. Beuther, A. Bik, T. Vasyunina, et al., *A&A*, **527**, A32, 2011.
17. I. I. Zinchenko, S.-Y. Liu, Y.-N. Su, K.-S. Wang, and Y. Wang, *ApJ*, **889**, 43, 2020.
18. I. Zinchenko, S.-Y. Liu, Y.-N. Su, S. V. Sali, et al., *ApJ*, **810**, 10, 2015.
19. W. O. Obonyo, S. L. Lumsden, M. G. Hoare, S. E. Kurtz, and S. J. D. Purser, *MNRAS*, **501**, 5197, 2021.
20. R. Fedriani, A. Caratti o Garatti, R. Cesaroni, J. C. Tan, et al., *A&A*, **676**, A107, 2023.
21. R. Cesaroni, L. Moscadelli, A. Caratti o Garatti, J. Eislöffel, et al., *A&A*, **680**, A110, 2023.
22. R. Cesaroni, L. Moscadelli, A. Caratti o Garatti, J. Eislöffel, et al., *A&A*, **683**, L15, 2024.
23. E. M. Howard, J. L. Pipher, and W. J. Forrest, *ApJ*, **481**, 327, 1997.
24. K. Fujisawa, Y. Yonekura, K. Sugiyama, H. Horiuchi, T. Hayashi, K. Hachisuka, N. Matsumoto, and K. Niinuma, *The Astronomer's Telegram*, **8286**, 2015.
25. S. V. Sali, I. I. Zinchenko, S.-Y. Liu, A. M. Sobolev, A. Aberfelds, and Y.-N. Su, *MNRAS*, **512**, 3215, 2022.
26. I. I. Zinchenko, S. Y. Liu, and Y. N. Su, *arXiv e-prints*, arXiv:2411.00116, 2024.
27. T. Hirota, R. Cesaroni, L. Moscadelli, K. Sugiyama, R. A. Burns, J. Kim, K. Sunada, and Y. Yonekura, *A&A*, **647**, A23, 2021.
28. G. Baek, J.-E. Lee, N. J. Evans, T. Hirota, Y. Aikawa, J.-h. Kang, J. Kim, and J. K. Jørgensen, *ApJL*, **954**, L25, 2023.

К вопросу о существовании кометного семейства Урана

Усанин В.С.

Казанский (Приволжский) федеральный университет, Казань, Россия

Ранее считалось общепризнанным деление комет в зависимости от их афелийных расстояний на семейства Юпитера, Сатурна, Урана и Нептуна. Современная классификация оставляет только семейство Юпитера, а семейства Сатурна, Урана и Нептуна заменены галлеевским типом. Переход от старой классификации к новой до сих пор вызывает критику. В качестве одной из характеристик динамической связи комет с планетами предлагался критерий Радзиевского-Тиссерана, который имеет смысл большой полуоси орбиты возмущающей планеты. В данной статье, продолжая предыдущую работу по семейству Сатурна, критерий Радзиевского-Тиссерана применен к кометам Кроммелина (27P), Стефана-Отерма (38P) и Темпеля-Тутля (55P) для проверки гипотезы об их принадлежности к семейству Урана. Ни одно значение критерия, вычисленное с учетом различных факторов, не лежит между большими полуосями орбит Сатурна и Нептуна. Таким образом, динамической связи этих комет с Ураном не выявлено. Подтверждается современная классификация комет.

Поступила в редакцию 04.10.2024 г. Принята в печать 14.11.2024 г.

Ключевые слова: динамика комет, семейство Урана, критерий Радзиевского-Тиссерана

Concerning the existence of the Uranus comet family

Usanin V.S.

Kazan (Volga region) Federal University, Kazan, Russia

Earlier, the division of comets depending on their aphelion distances into the planetary families of Jupiter, Saturn, Uranus and Neptune was regarded as undoubted. The modern classification system retains only the Jupiter family, and the families of Saturn, Uranus and Neptune are replaced by the Halley type. The transition from the old classification system to the new one still raises criticism. The Radzievskij-Tisserand criterion, which fits the orbital semimajor axis of the perturbing planet, was proposed as a measure of the dynamical relation of comets to planets. In the present paper, continuing the previous work on the Saturn family, the Radzievskij-Tisserand criterion is applied to comets 27P/Crommelin, 38P/Stephan-Oterma, and 55P/Tempel-Tuttle for the evaluation of the hypothesis that they belong to the Uranus family. No one value of the criterion calculated considering different factors lies between the Saturn and Neptune's orbital semimajor axes. So, no dynamical relation of these comets to Uranus is revealed. The modern comet classification system seems to be right.

Received 04.10.2024. Accepted 14.11.2024.

Keywords: cometary dynamics, Uranus family, Radzievskij-Tisserand criterion

DOI: 10.51194/INASAN.2024.9.2.003

1. Introduction

Earlier, the division of comets into the families of Jupiter, Saturn, Uranus and Neptune [1] was regarded as undoubted. The modern classification system [2] retains only the Jupiter family, and comets with larger aphelion distances belong to the Halley type. Because the numerical integration does not allow separation of perturbations from individual planets, the transition from the old classification system to the new one still raises criticism (see [3] for a review).

Within the framework of the circular restricted three-body problem, the Tisserand constant expressed as a function of the orbital elements of the tertiary body (a comet) and the orbital semimajor axis of the secondary body (a planet) with respect to the primary body (the sun) is a kind of approximate conservation law. Radzievskij assumed values of the Tisserand constant at two different times (apparitions of the comet) equal and so expressed the constant quantity, which fits the orbital semimajor axis of the perturbing planet:

$$A = \left(\frac{2\sqrt{(1+e_1)q_1} \cos i_1 - 2\sqrt{(1+e_2)q_2} \cos i_2}{a_2^{-1} - a_1^{-1}} \right)^{2/3},$$

where q , e , i , and $a = q/(1-e)$ are the perihelion distance, the eccentricity, the inclination, and the semimajor axis of the cometary orbit, respectively, and 1 and 2 indices denote the two different apparitions of the same comet. The Radzievskij-Tisserand criterion [4] is a measure of the dynamical relation of comets to planets.

In my previous research [5], I applied the Radzievskij-Tisserand criterion to a presumed Saturn-family comet and revealed some practical aspects of its use. In the present paper I apply the Radzievskij-Tisserand criterion to presumed Uranus-family comets.

Table 1: Values of A in AU calculated for pairs of apparitions of 27P using the orbital elements from the JPL NASA’s Small-Body Database Lookup.

	1818	1873	1928	1956
2002	47.96	6.35	6.50	6.36
1956	2.03	6.32	8.57	
1928	2.64	5.82		
1873	3.51			

Table 2: Values of A in AU calculated for pairs of apparitions of 27P from the orbital elements integrated using the JPL NASA’s Horizons Web Application backward from 2002.

	1818	1873	1928	1956
2002	8.34	6.35	6.50	6.36
1956	2.68	6.32	8.56	
1928	3.73	5.81		
1873	4.62			

2. Methods and results of calculations

The aphelion distance $Q = 17.45$ AU of comet 27P/Crommelin is much closer to the orbital semimajor axis of Uranus $a_U = 19.19$ AU than to that of Saturn what makes it a presumed Uranus-family comet. The JPL NASA’s Small-Body Database Lookup [6] provides the orbital elements for 5 apparitions of this comet from 1818 to 2002. The values of the Radzievskij-Tisserand criterion A for all possible pairs of apparitions calculated from these elements are present in Table 1. We can see that no one value of A is in the exclusive proximity to the orbital semimajor axis of Uranus and, even more, no one lies between those of Saturn $a_S = 9.58$ AU and of Neptune $a_N = 30.07$ AU. To eliminate possible effect of observational errors on the values of A , another set of the orbital elements integrated using the JPL NASA’s Horizons Web Application backward from 2002 to the same times is also applied in the calculations. The results are present in Table 2. To eliminate possible effect of nongravitational forces on the values of A , the third set of the orbital elements integrated using the JPL NASA’s Horizons telnet interface without the nongravitational parameters backward from 2002 to the same times is also applied in the calculations. The results are present in Table 3. No one value of A calculated from the integrated orbital elements is more than the Saturn’s orbital semimajor axis.

The aphelion distance $Q = 20.99$ AU of comet 38P/Stephan-Oterma is much closer to the orbital semimajor axis of Uranus than to that of Neptune, so it is also a presumed Uranus-family comet. The JPL NASA’s Small-Body Database Lookup provides the orbital elements for 3 apparitions of this comet from 1942 to 2018. The calculations of A for all possible pairs of apparitions from these elements and from the orbital elements integrated backward from 2018 to the same times with and without the nongravitational parameters give matching figures. Their results are present in Table 4. No one value of A for 38P is more than the Jupiter’s orbital semimajor axis.

Comet 55P/Tempel-Tuttle is widely known as the parent body of the Leonid meteor shower and has now the aphelion distance $Q = 19.70$ AU. Interestingly, it is the only comet originally listed [1] as a Uranus-family comet with $Q = 19.14$ AU then. The JPL NASA’s Small-Body Database Lookup provides the orbital elements for 5 apparitions of this comet from 1366 to 1998. The values of A for all possible pairs of apparitions calculated from these elements are present in Table 5. JPL NASA’s Horizons allows backward integration only to 1599, so in further calculations 4 apparitions from 1699 are considered. The values of A calculated from the orbital elements

Table 3: Values of A in AU calculated for pairs of apparitions of 27P from the orbital elements integrated using the JPL NASA’s Horizons telnet interface without the nongravitational parameters backward from 2002.

	1818	1873	1928	1956
2002	8.32	6.34	6.50	6.35
1956	2.68	6.32	8.55	
1928	3.73	5.82		
1873	4.62			

Table 4: Values of A in AU calculated for pairs of apparitions of 38P using the orbital elements from the JPL NASA’s Small-Body Database Lookup and integrated using the JPL NASA’s Horizons with and without the nongravitational parameters backward from 2018.

	1867	1942
2018	4.32	5.16
1942	4.77	

Table 5: Values of A in AU calculated for pairs of apparitions of 55P using the orbital elements from the JPL NASA’s Small-Body Database Lookup.

	1366	1699	1865	1965
1998	2.50	4.79	–	6.23
1965	4.30	5.26	2.95	
1865	9.12	8.02		
1699	7.49			

Table 6: Values of A in AU calculated for pairs of apparitions of 55P from the orbital elements integrated using the JPL NASA’s Horizons Web Application backward from 1998.

	1699	1865	1965
1998	4.77	–	6.03
1965	5.19	2.95	
1865	7.76		

Table 7: Values of A in AU calculated for pairs of apparitions of 55P from the orbital elements integrated using the JPL NASA’s Horizons telnet interface without the nongravitational parameters backward from 1998.

	1699	1865	1965
1998	4.73	–	6.07
1965	5.17	2.94	
1865	7.71		

integrated backward from 1998 are present in Table 6 and those without the nongravitational parameters are present in Table 7. No one value of A for 55P is more than the Saturn’s orbital semimajor axis, and one pair of apparitions gives insistently a complex number (denoted by dashes) for A .

3. Conclusions

No one pair of apparitions of 27P, 38P, and 55P, presumed Uranus-family comets, gives a value of the Radzievskij-Tisserand criterion between the Saturn and Neptune’s orbital semimajor axes. So, these comets have no dynamical relation to Uranus. The new comet classification retaining only Jupiter family and Halley type seems to be right.

References

1. M. Roller, *Astronomische Nachrichten*, **75**, 331, 1870.
2. A. Carusi, L. Kresak, E. Perozzi, and G. B. Valsecchi, *Astron. and Astrophys.*, **187**, 899, 1987.
3. B. G. Marsden, *Plan. and Space Sci.*, **57**, 1098, 2009.
4. V. P. Tomanov, *Kometnyj Tsirkulyar*, **328**, 1984.
5. V. S. Usanin, *INASAN Science Reports*, **5**, 65, 2020.
6. J. D. Giorgini, D. K. Yeomans, A. B. Chamberlin, P. W. Chodas, et al., in *AAS/Division for Planetary Sciences Meeting Abstracts #28*, **28**, 25.04 (1996).

Динамические и физические параметры астероидов, сближающихся с Землей, по данным наблюдений на телескопе СБГ

Кузнецов Э.Д., Галиуллин М.И., Гламазда Д.В., Вибе Ю.З.

Уральский федеральный университет, Екатеринбург, Россия

Представлены результаты позиционных и многоцветных фотометрических наблюдений астероидов, сближающихся с Землей (АСЗ), на телескопе СБГ Коуровской астрономической обсерватории Уральского федерального университета в 2023–2024 гг. По результатам позиционных наблюдений были получены элементы орбит 26 астероидов, включая потенциально опасный астероид (439437) 2013 NK4 и семь АСЗ размером более 1 км. Кроме того, оценены периоды осевого вращения астероидов (154029) 2002 CY46 и (154244) 2002 KL6 по фотометрическим наблюдениям. Из многоцветных фотометрических наблюдений в фильтрах V, R и I получены показатели цвета для 15 астероидов. Наблюдения с помощью телескопа SBG позволяют определить как динамические, так и физические характеристики АСЗ.

Поступила в редакцию 12.10.2024 г. Принята в печать 14.11.2024 г.

Ключевые слова: астероиды, сближающиеся с Землей; позиционные наблюдения; фотометрические наблюдения; орбиты; периоды вращения; показатели цвета

Dynamic and physical parameters of near-Earth asteroids from SBG telescope observations

Kuznetsov E.D., Galiullin M.I., Glamazda D.V., Wiebe Yu.S.

Ural Federal University, Yekaterinburg, Russia

We present results of astrometric and multicolor photometric observations of near-Earth objects (NEOs) at the SBG telescope of the Kourovka Astronomical Observatory of the Ural Federal University in 2023–2024. We improved orbital elements for 26 asteroids from astrometric observations, including potential hazardous asteroid (439437) 2013 NK4 and seven NEOs with diameters more than 1 km. Furthermore, we estimated the axial rotation periods of the asteroids (154029) 2002 CY46 and (154244) 2002 KL6 from photometric observations. We obtained color indices for 15 asteroids from multicolor photometric observations in filters V, R, and I. Observations with the SBG telescope make it possible to determine both the dynamic and physical characteristics of NEOs.

Received 12.10.2024. Accepted 14.11.2024.

Keywords: near-Earth objects; astrometry; photometry; orbits; rotation periods; color indices

DOI: 10.51194/INASAN.2024.9.2.004

1. Introduction

Observations of near-Earth objects (NEOs) have a few features that distinguish them from main belt asteroids. The periods of visibility during which NEOs are accessible to small and medium-sized ground-based telescopes are irregular. The smaller the size of an NEO, the longer the time intervals between its appearances on average, and the shorter the time intervals that allow observations to be made. In the case of close approaches of asteroids to the Earth, it becomes possible to observe small objects with diameters of a few tens or hundreds of meters, but the area of the Earth's surface from which observations can be made is reduced. Each occurrence of NEOs becomes a unique transient phenomenon that provides new information characterizing the dynamic and physical properties of the asteroid. We present results of astrometric and multicolor photometric observations of near-Earth asteroids at the SBG telescope of the Kourovka Astronomical Observatory of the Ural Federal University (KAO UrFU) in 2023–2024. A description of the instruments and light-receiving equipment is given in Section 2. Section 3 presents the results of positional observations. In Section 4, the periods of axial rotation are estimated. We derived the axis ratio a/b of the observed NEOs in Section 5. Section 6 presents the results of multicolor photometric observations.

2. SBG telescope

Observations of NEOs were carried out using the SBG telescope of the KAO UrFU. The main parameters of the SBG telescope and their light-receiving equipment are given in Table 1. For astrometric observations, the R filter was used; and for photometric observations, the V, R, I filters were used.

3. Accuracy of astrometric observations

Astrometric observations processing was performed using the IzmCCD¹ software [1]. Based on the results of positional observations, the orbits of asteroids that were observed with the SBG telescope in 2023–2024 were

¹<http://izmccd.puldb.ru/>

Table 1: Basic parameters of the SBG telescope.

Parameter	SBG
Optical system	Schmidt
Mirror diameter, m	0.4
Focal length, m	0.8
CCD camera	Apogee Alta U32
Pixel size, μm	6.8×6.8
Scale, arcsec/pixel	1.8
Field of view, arcmin	65×44

Table 2: Accuracy of astrometric observations based on the improved orbits.

NEO	σ , arcsec	σ_r , au	σ_v , au day $^{-1}$
(1685) Toro	0.44	7.3×10^{-8}	2.9×10^{-10}
(2063) Bacchus	0.48	3.4×10^{-8}	1.0×10^{-9}
(4769) Castalia	0.57	4.6×10^{-8}	1.6×10^{-9}
(21374) 1997 WS22	0.36	3.4×10^{-8}	7.6×10^{-10}
(25330) 1999 KV4	0.42	4.0×10^{-8}	6.5×10^{-10}
(68548) 2001 XR31	0.32	5.6×10^{-8}	1.3×10^{-9}
(86667) 2000 FO10	0.36	3.4×10^{-8}	7.0×10^{-10}
(98943) 2001 CC21	0.34	2.2×10^{-8}	3.7×10^{-10}
(139622) 2001 QQ142	0.37	2.6×10^{-8}	6.4×10^{-9}
(141851) 2002 PM6	0.44	1.2×10^{-7}	1.0×10^{-9}
(152787) 1999 TB10	0.37	5.6×10^{-8}	1.3×10^{-9}
(154029) 2002 CY46	0.34	7.3×10^{-8}	2.5×10^{-9}
(154244) 2002 KL6	0.29	7.5×10^{-9}	2.4×10^{-10}
(164121) 2003 YT1	0.38	1.4×10^{-8}	1.2×10^{-9}
(187026) 2005 EK70	0.34	3.1×10^{-8}	1.6×10^{-9}
(271480) 2004 FX31	0.35	3.9×10^{-8}	7.7×10^{-10}
(349507) 2008 QY	0.26	1.9×10^{-8}	6.3×10^{-10}
(417264) 2006 AT2	0.25	4.4×10^{-8}	1.3×10^{-9}
(422787) 2001 WS1	0.27	3.3×10^{-8}	1.3×10^{-9}
(439437) 2013 NK4	0.38	7.9×10^{-8}	6.3×10^{-9}
(458732) 2011 MD5	0.23	2.0×10^{-8}	6.3×10^{-10}
(518635) 2008 HO3	0.29	3.0×10^{-8}	7.9×10^{-10}
2004 UV1	0.34	6.9×10^{-8}	1.6×10^{-9}
2008 TB27	0.37	1.1×10^{-7}	5.5×10^{-9}

improved using the IDA software package [2]. Based on the improved orbital elements, the root-mean-square errors σ of the differences ($O - C$) as the root-mean-square errors of the coordinates and velocity components σ_r and σ_v were obtained. The results are given in Table 2, where σ is the root-mean-square error of the differences ($O - C$) for all observations used to improve the orbit. The accuracy of determining the coordinates of NEOs presented in Table 2 according to observations with the SBG telescope is: in ($O - C$) — $0.2'' - 0.6''$, in coordinates — $10^{-7} - 10^{-9}$ au, in velocity components — $10^{-9} - 10^{-10}$ au day $^{-1}$, which is sufficient to solve the problem of operational tracking of objects.

4. Periods of rotation

The initial processing of photometric observations was carried out using the AM:PM software developed at the Kourvka Astronomical Observatory of UrFU. Typically, photometric observations with the SBG telescope are carried out for objects brighter than $16.5^m - 17.0^m$, which ensures the accuracy of determining stellar magnitude is no worse than 0.05^m [3].

To determine the rotation periods of asteroids from phase lightcurves, magnitudes in various filters were normalized to the R filter. When constructing phase lightcurves to take into account the dependence of the asteroid's brightness on the phase angle, the parameters of two- or three-parameter models were determined using the *Online calculator for H, G1, G2 photometric system*² [4, 5, 6]. The construction of phase lightcurves and

²<http://h152.it.helsinki.fi/HG1G2/>

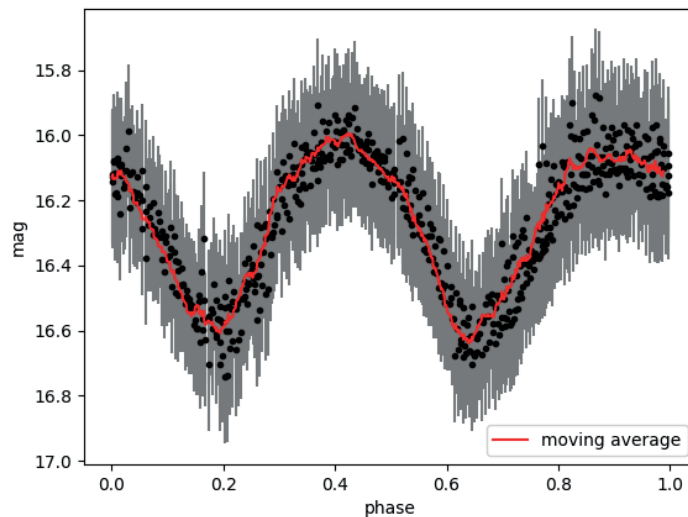


Figure 1: Phase lightcurve of the asteroid (154244) 2002 KL6. The red line is the moving average.

Table 3: Axis ratios of NEOs.

NEO	a/b
(1685) Toro	1.139 ± 0.021
(2063) Bacchus	1.168 ± 0.007
(4769) Castalia	1.295 ± 0.053
(21374) 1997 WS22	1.100 ± 0.006
(25330) 1999 KV4	1.111 ± 0.012
(68548) 2001 XR31	1.047 ± 0.009
(86667) 2000 FO10	1.094 ± 0.001
(152787) 1999 TB10	1.207 ± 0.028
(139622) 2001 QQ142	1.107 ± 0.010
(141851) 2002 PM6	1.108 ± 0.005
(154029) 2002 CY46	1.095 ± 0.012
(154244) 2002 KL6	1.275 ± 0.005
(164121) 2003 YT1	1.056 ± 0.005
(187026) 2005 EK70	1.203 ± 0.002
(271480) 2004 FX31	1.089 ± 0.006
(349507) 2008 QY	1.352 ± 0.016
(417264) 2006 AT2	1.304 ± 0.010
(439437) 2013 NK4	1.228 ± 0.007
(458732) 2011 MD5	1.215 ± 0.012
(518635) 2008 HO3	1.173 ± 0.012

estimation of the axial rotation period P were performed in the online system *Period search service*³ using the Lafleur-Kinman method [7]. Example of phase lightcurve of the asteroid (154244) 2002 KL6 is shown in Fig. 1. The ordinate axis shows the absolute magnitudes in the R filter H_R . We estimated the periods P of axial rotation of two asteroids (154029) 2002 CY46 and (154244) 2002 KL6: $P_{154029} = 2.6^{\text{h}} \pm 0.1^{\text{h}}$ and $P_{154244} = 4.6^{\text{h}} \pm 0.1^{\text{h}}$. The results are consistent with the data on asteroid rotation periods contained in *the Asteroid Light Curve Database of the Minor Planet Center* (ALCDEF⁴), within the limits of determination errors: $P_{154029} = 2.554^{\text{h}} \pm 0.001^{\text{h}}$ [8] and $P_{154244} = 4.610^{\text{h}} \pm 0.001^{\text{h}}$ [9].

³<http://scan.sai.msu.ru/lk/>

⁴<https://alcdef.org/>

Table 4: Color indices comparison.

$V - R$	$V - I$	$R - I$	Reference
(1685) Toro			
0.524 ± 0.040	0.878 ± 0.014	0.354 ± 0.026	SBG
0.489 ± 0.024	0.869 ± 0.027	–	[14]
(86667) 2000 FO10			
0.445 ± 0.034	0.758 ± 0.027	0.313 ± 0.047	SBG
0.480 ± 0.030	–	–	[15]
(154244) 2002 KL6			
0.456 ± 0.002	0.765 ± 0.003	0.309 ± 0.004	SBG
0.460 ± 0.030	0.750 ± 0.040	–	[16]
(271480) 2004 FX31			
0.432 ± 0.066	0.776 ± 0.027	0.344 ± 0.091	SBG
0.420 ± 0.030	0.750 ± 0.040	–	[17]

Table 5: Color indices of NEOs.

NEO	$V - R$	$V - I$	$R - I$
(2063) Bacchus	0.461 ± 0.036	0.780 ± 0.024	0.319 ± 0.022
(4769) Castalia	0.456 ± 0.186	0.949 ± 0.276	0.494 ± 0.416
(21374) 1997 WS22	0.461 ± 0.024	0.871 ± 0.037	0.411 ± 0.027
(25330) 1999 KV4	0.359 ± 0.013	0.680 ± 0.011	0.321 ± 0.009
(139622) 2001 QQ142	0.449 ± 0.044	0.814 ± 0.038	0.365 ± 0.047
(152787) 1999 TB10	0.311 ± 0.036	0.866 ± 0.062	0.554 ± 0.098
(154029) 2002 CY46	0.480 ± 0.021	0.830 ± 0.013	0.351 ± 0.024
(164121) 2003 YT1	0.481 ± 0.022	0.659 ± 0.028	0.178 ± 0.019
(187026) 2005 EK70	0.415 ± 0.046	0.752 ± 0.047	0.337 ± 0.033
(417264) 2006 AT2	0.341 ± 0.042	0.813 ± 0.035	0.472 ± 0.077
(458732) 2011 MD5	0.386 ± 0.044	0.706 ± 0.050	0.320 ± 0.063

5. Axis ratio

We derived the axis ratio a/b of the observed NEOs. To correct peak-to-peak lightcurve amplitude values, we taken into account the phase angle correction as follows:

$$\Delta m(\alpha = 0^\circ) = \frac{\Delta m(\alpha)}{1 + s\alpha}, \quad (1)$$

$$\frac{a}{b} \geq 10^{(0.4\Delta m(\alpha))/(1+s\alpha)}, \quad (2)$$

where $\Delta m(\alpha)$ is the lightcurve amplitude at phase angle α and $s = 0.03 \text{ mag deg}^{-1}$ is the slope correlating the amplitude and the phase angle [10, 11, 12]. Table 3 gives the axis ratios a/b of the observed NEOs. NEOs for which the ratio a/b is obtained from the full lightcurve are shown in bold. For other objects, the ratio estimates are obtained using a partial lightcurves. The average axis ratio for small near-Earth objects is $1.31 - 1.33$ [13]. The results obtained in this paper are consistent with this estimate of the average value of the ratio.

6. Color indices

Tables 4 and 5 show estimates of the color indices $V - R$, $V - I$, and $R - I$ of NEOs based on the results of observations using the SBG. The Table 4 compares the color indices obtained from the SBG telescope observations with data from other works. The estimates of color indices coincide within the standard deviation. The Table 5 contains estimates of color indices for which there are no data in the ALCDEF database.

7. Conclusions

The results obtained show that observations with the SBG telescope of the Kourovka Astronomical Observatory of UrFU make it possible to determine both the dynamic and physical characteristics of NEOs. Obtaining improved orbital elements makes it possible to conduct detailed studies of the orbital evolution of NEOs. Photometric observations allow us to determine axial rotation periods and characterize the shape of asteroids through an estimate of the rotation ellipsoid axis ratio. Multicolor photometry gives reliable estimates of color indices $V - R$, $V - I$, and $R - I$.

Funding

The work was supported by the Ministry of Science and Higher Education of the Russian Federation, project FEUZ-2023-0019.

The SBG telescope is part of the Unique Scientific Installation “Kourovka Astronomical Observatory”.

References

1. I. S. Izmailov, M. L. Khovrichева, M. Y. Khovrichев, O. V. Kiyayeva, et al., *Astronomy Letters*, **36**, 349, 2010.
2. T. Y. Galushina, L. E. Bykova, O. N. Letner, and A. P. Baturin, *Astronomy and Computing*, **29**, 100301, 2019.
3. E. D. Kuznetsov, Y. Z. Wiebe, D. V. Glamazda, G. T. Kaiser, V. V. Krushinsky, M. S. Kryuchkov, S. A. Naroenkov, and A. S. Perminov, *Astronomy Reports*, **68**, 672, 2024.
4. K. Muinonen, I. N. Belskaya, A. Cellino, M. Delbò, A.-C. Levasseur-Regourd, A. Penttilä, and E. F. Tedesco, *Icarus*, **209**, 542, 2010.
5. D. A. Oszkiewicz, K. Muinonen, E. Bowell, D. Trilling, A. Penttilä, T. Pieniluoma, L. H. Wasserman, and M. T. Enga, *Journal of Quantitative Spectroscopy and Radiative Transfer*, **112**, 1919, 2011.
6. A. Penttilä, V. G. Shevchenko, O. Wilkman, and K. Muinonen, *Plan. and Space Sci.*, **123**, 117, 2016.
7. J. Lafler and T. D. Kinman, *Astrophys. J. Supp.*, **11**, 216, 1965.
8. B. A. Skiff, K. P. McLelland, J. J. Sanborn, P. Pravec, and B. W. Koehn, *Minor Planet Bulletin*, **46**, 458, 2019.
9. B. D. Warner, *Minor Planet Bulletin*, **50**, 304, 2023.
10. V. Zappala, A. Cellino, A. M. Barucci, M. Fulchignoni, and D. F. Lupishko, *Astron. and Astrophys.*, **231**, 548, 1990.
11. P. J. Gutiérrez, B. J. R. Davidsson, J. L. Ortiz, R. Rodrigo, and M. J. Vidal-Nuñez, *Astron. and Astrophys.*, **454**, 367, 2006.
12. A. Thirouin, N. Moskovitz, R. P. Binzel, E. Christensen, et al., *Astron. J.*, **152**, 163, 2016.
13. J. A. Sanchez, V. Reddy, A. Thirouin, W. F. Bottke, et al., *Planetary Science Journal*, **5**, 131, 2024.
14. C.-H. Lin, W.-H. Ip, Z.-Y. Lin, Y.-C. Cheng, H.-W. Lin, and C.-K. Chang, *Plan. and Space Sci.*, **152**, 116, 2018.
15. D. Polishook and N. Brosch, *Icarus*, **194**, 111, 2008.
16. N. Erasmus, M. Mommert, D. E. Trilling, A. A. Sickafoose, C. van Gend, and J. L. Hora, *Astron. J.*, **154**, 162, 2017.
17. T. Hromakina, M. Birlan, M. A. Barucci, M. Fulchignoni, et al., *Astron. and Astrophys.*, **656**, A89, 2021.

Анализ динамических параметров метеорного комплекса Канкрид и его дрейфового движения

Сергиенко М.В.¹, Нефедьев Ю.А.¹, Андреев А.О.^{1,2}

¹Казанский федеральный университет, Казань, Россия

²Казанский государственный энергетический университет, Казань, Россия

Работа посвящена исследованию динамических параметров метеороидного комплекса Канкриды и его дрейфового движения. Согласно современным представлениям, малые тела Солнечной системы благодаря своей малой массе, не изменили свои физико-химические свойства и состав. Изучение астрофизических характеристик малых небесных тел, в особенности метеороидов и связанных с ними метеорных потоков, дают ценные сведения об эволюции Солнечной системы. Отдельно для метеорных баз данных, созданных по разным каталогам метеорных орбит, определены радианты, площадь радиации, уточнены параметры суточного смещения. Определены резонансы с Юпитером. Построено и проанализировано распределение координат радиантов метеороидного комплекса Канкриды в зависимости от долготы Солнца. Анализ распределения показывает, что северная и южная ветви метеороидного комплекса Канкриды наблюдаются в схожие даты, наблюдается хорошее согласие по данным скоростей для разных метеорных баз и с литературными источниками, локализация радиантов происходит по склонению и прямому восхождению. Сделан вывод, что эволюционный механизм образования ветвей комплекса Канкрид, разный. Показано, что южная и северная ветвь комплекса Канкриды образовались при различных эволюционных условиях, как, например, при вторичном распаде родительского тела.

Поступила в редакцию 05.10.2024 г. Принята в печать 14.11.2024 г.

Ключевые слова: метеороидный поток, радиант, резонанс

Analysis of the dynamic parameters of the Cancrids meteor shower and its drift motion

Sergienko M.V.¹, Nefedyev Y.A.¹, Andreev A.O.^{1,2}

¹Kazan Federal University, Kazan, Russia

²Kazan State Power Engineering University, Kazan, Russia

The work is devoted to the study of the dynamic parameters of the Cancrids meteoroid complex and its drift motion. According to modern concepts, small bodies of the Solar System, due to their low mass, have not changed their physical and chemical properties and composition. The study of the astrophysical characteristics of small celestial bodies, especially meteoroids and associated meteor showers, provides valuable information about the evolution of the solar system. Separately for meteor databases created using different meteor orbit catalogues, radiant and radiation areas were determined, and the parameters of daily shift were refined. Resonances with Jupiter were determined. The distribution of radiant coordinates of the Cancrids meteoroid complex was constructed and analyzed depending on the longitude of the Sun. The distribution analysis shows that the northern and southern branches of the Cancrids meteoroid complex are observed on similar dates, there is good agreement in the velocity data for different meteor bases and with literary sources, the localization of radiants occurs by declination and right ascension. It is concluded that the evolutionary mechanism of formation of branches of the Cancrids complex is different. It is shown that the southern and northern branches of the Cancrids complex were formed under different evolutionary conditions, such as the secondary disintegration of the parent body.

Received 05.10.2024. Accepted 14.11.2024.

Keywords: meteor showers, radiants, resonance

DOI: 10.51194/INASAN.2024.9.2.005

1. Introduction

One of the important tasks of astronomy and astrophysics is the study of the solar system, specifically small bodies such as comets, asteroids, and meteoroids. According to the modern concept, comets, asteroids, and meteoroids contain the information about the original matter that participated in the formation of the solar system. The major part of small bodies has not changed its physical and chemical properties and composition, as they are objects with small masses. Therefore, by studying the astrophysical characteristics of small celestial bodies, especially meteoroids and the showers that produce them, we may get valuable insights into the evolution of the solar system.

The Cancrids meteor complex is a small shower that has been confirmed by observations. The shower has two branches, the Northern Cancrids NCC, number 96 on the Meteor Data Center database, and the Southern Cancrids SCC, number 97. There is no parent body associated with the shower. It is observed in January. The shower is poorly studied in terms of its evolution and structural parameters.

2. Methods

Tables 1 and 2 present the elements of the mean orbits of the Cancrids meteor complex. Tables 1 and 2 show the elements of the mean orbit of the shower taken from the literature. Table 3 provides the elements of the Cancrids

Table 1: Elements of the shower's mean orbits.

Branch of the Cancrids	V (km/s)	RA $^\circ$	DE $^\circ$	L°	a (AU)	e	Reference
NCC	28.2	127.6	21.5	296.9	2.408	0.835	[1]
SCC	27.9	117.5	16.1	287.1	2.298	0.399	[1]
NCC	27.0	127.6	21.5	296.0	2.260	0.810	[2]
NCC	29.9	131.4	17.6	299.0	–	–	[3]
SCC	26.8	134.1	10.1	296.3	2.114	0.761	[4]
SCC	28.7	131.5	10.6	298.0	–	–	[5]

averaged orbits for both branches calculated by the authors. We calculated the elements of the mean orbits of the Cancrids using our meteor data based on the EDMOND, CAMS, and SonatoCo catalogues.

It is important to note that the Cancrids complex, according to the Tisserand's parameter T relative to Jupiter, lies between the cometary and asteroidal types, i.e., T is about 3, but according to the values of the parameter T from some of catalogues, the shower is more likely to be of asteroidal type.

Table 2: Elements of the shower's mean orbits — our calculations.

Shower, IAU No.	Catalogue	$a \pm \sigma$ (AU)	$e \pm \sigma$	$q \pm \sigma$ (AU)	$i^\circ \pm \sigma^\circ$	$\pi^\circ \pm \sigma^\circ$	$T \pm \sigma$
NCC No. 96	EDMOND	2.073 ± 0.387	0.780 ± 0.043	0.437 ± 0.072	3.127 ± 1.262	222.547 ± 5.195	3.264 ± 0.458
	CAMS	2.224 ± 0.656	0.801 ± 0.058	0.412 ± 0.047	2.481 ± 1.709	225.246 ± 7.637	3.126 ± 0.381
	SonatoCo	2.349 ± 0.201	0.813 ± 0.035	0.420 ± 0.080	2.481 ± 1.005	225.246 ± 4.562	3.101 ± 0.528
SCC No. 97	EDMOND	2.063 ± 0.221	0.788 ± 0.028	0.435 ± 0.060	7.209 ± 3.761	230.212 ± 5.115	3.533 ± 0.452
	CAMS	2.063 ± 0.328	0.812 ± 0.061	0.435 ± 0.005	5.676 ± 2.321	233.705 ± 7.600	3.076 ± 0.316
	SonatoCo	2.257 ± 0.220	0.821 ± 0.030	0.374 ± 0.061	5.677 ± 1.320	233.704 ± 5.102	3.300 ± 0.876

3. Results

There are very few photo-derived orbits for the Cancrids meteoroid complex. Therefore, the study additionally involved television observations as well, e.g. TV catalogues SonatoCo, CAMS, EDMOND with sufficient orbit statistics. The minimum stellar magnitude in catalogues for the Cancrids complex is $+3.4^m$. The error in determining the geocentric velocity is approximately 1.0 km/s.

Fig. 1 shows the distribution of the RA $^\circ$ and DE $^\circ$ radiant coordinates of the Cancrids meteoroid complex as a function of the Sun's longitude L° . Radiants of the northern branch (NCC) according to the SonatoCo catalogue — black squares, radiants of the southern branch (SCC) — red dots. For the CAMS catalogue, radiants for the NCC — green triangles, radiants of the SCC — blue rhombuses. EDMOND catalogue: radiants of the NCC and SCC — blue and pink triangles, respectively. The black lines represent correlation linear dependencies.

The analysis of Fig. 1 shows that the NCC and SCC are observed on similar dates, there is good agreement in velocities (see Table 1 and 2), and the radiants are localized by declination and right ascension. It can be seen that DE $^\circ$ values are higher for the northern branch compared to the southern one for all the catalogues used, while RA $^\circ$ values are lower. The correlation coefficients between linear dependencies of RA $^\circ$ and DE $^\circ$ and the

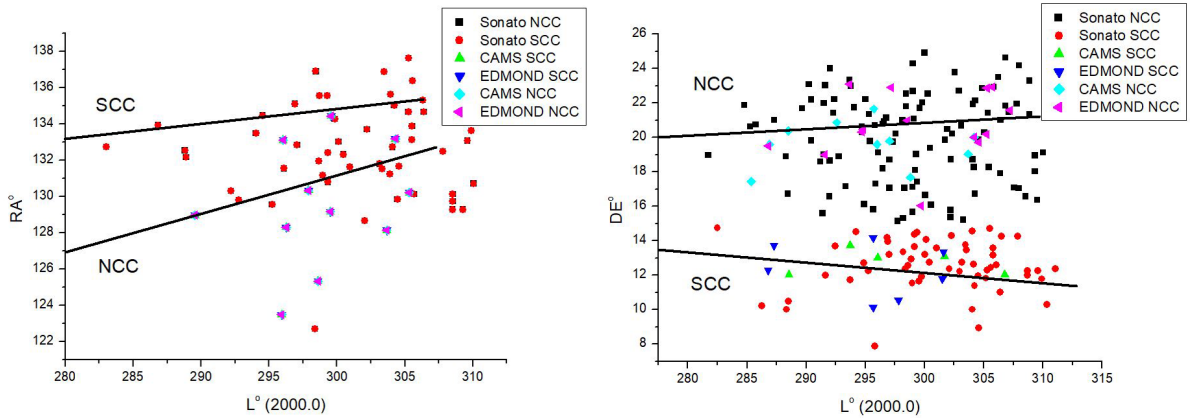


Figure 1: Radiant coordinates of the Cancrids as a function of solar longitude.

Table 3: Data on velocities and radiants for each of the branches of the Cancrids complex.

Branch	V_g , km/s	V_h , km/s	RA $^\circ$	DE $^\circ$	dRA°	dDE°	S_r
NCC	27.10 ± 3.40	37.41 ± 1.31	129.80 ± 2.71	19.83 ± 2.70	0.170 ± 0.032	0.033 ± 0.031	$7^\circ \times 6^\circ$
SCC	28.00 ± 3.10	36.80 ± 2.21	133.52 ± 2.10	12.31 ± 1.70	0.021 ± 0.040	-0.020 ± 0.041	$4^\circ \times 3^\circ$

stellar magnitude of the meteors were determined. Dependencies of RA $^\circ$ right ascension and DE $^\circ$ declination on the stellar magnitude of the meteors were found to be different in sign.

The coordinates of the radiants and their diurnal variations for each branch were determined both from the coordinates of individual radiants and from the coordinates averaged to 1 $^\circ$ of solar longitude. Table 3 shows the results obtained, namely, the velocity and radiant data for the Cancrids for each branch separately. Table 3 shows the velocities V_g and V_h in km/s, right ascension RA $^\circ$ and declination DE $^\circ$, taking into account their errors dRA° and dDE° , and the radiant area S_r .

The diurnal displacement of the radiants dRA , dDE for each branch was determined from the individual coordinates RA and DE according to the formulas:

$$RA_i^* = RA_i - (L_i - L_0) \cdot dRA, \quad (1)$$

$$DE_i^* = DE_i - (L_i - L_0) \cdot dDE, \quad (2)$$

where RA_i , DE_i are the individual coordinates of the radiants. The values of dRA , dDE were found by correlation analysis using the linear dependencies RA(L), DE(L) plotted by straight lines in Fig. 1.

The results shown in Tables 1–3 are in good agreement. The velocity values are close, but right ascension RA $^\circ$ and declination DE $^\circ$ are different, and the radiation area is also different. Most likely, the branches of the complex were formed under different evolutionary conditions and probably at different times. The SCC branch has smaller values of radiation area and RA $^\circ$ right ascension and DE $^\circ$ declination, so it is very likely that the SCC form as a result of disintegration of the parent body. Since more observational statistics is available for the SCC, the diurnal radiant drift is more reliably determined compared to NCC.

4. Conclusion

The Cancrids meteoroid complex is subject to strong gravitational perturbations from Jupiter during its motion, as its orbital period is approximately 4 years. The southern branch of the complex (SCC) falls into significant 2:1 and 1:1 resonances with Jupiter. The obtained radiants for both branches of the shower have a clear agreement with the data obtained by other authors (Table 1). The values of the diurnal variations of the radiants were refined, and the areas of radiation were determined. It is shown that it is possible that both branches (SCC and NCC) formed under different evolutionary conditions, such as secondary disintegration of the parent body.

Funding

This work was supported by Russian Science Foundation, grant no. 24-22-00260.

References

1. S. Yasuo, *WGN, Journal of the International Meteor Organization*, **50**, 38, 2022.
2. O. Bel'kovich, M. Ishmukhametova, and N. Suleimanov, *Solar System Research*, **35**, 400, 2001.
3. Z. Sekanina, *Icarus*, **27**, 265, 1976.
4. S. Molau and J. Rendtel, *WGN, Journal of the International Meteor Organization*, vol. 37, no. 4, p. 98-121, **37**, 98, 2009.
5. S. V. M. Clube, *Vistas in Astronomy*, **39**, 673, 1995.

Перспективы развития метеорных радиолокационных наблюдений в Казанском федеральном университете

Коротышкин Д.В., Шерстюков О.Н., Валиуллин Ф.С.

Казанский федеральный университет, Казань, Россия

Статья посвящена модернизации метеорного радара на базе системы SKiYMET в Казанском федеральном университете. Целью модернизации является повышение точности радиолокационных наблюдений за метеорами. В ходе модернизации количество антенн увеличилось с 5 до 12, а размеры измерительных баз были расширены до 220 м на 150 м. Эти изменения значительно улучшили точность измерений угловых координат, достигая значений не хуже 0.3 градуса. Также представлены статистические данные мониторинга, проведенного в 2023 г., по которым количество зарегистрированных метеоров с оценкой скорости метеора варьировалось от 15000 до 40000 в сутки. На основе анализа выявленных проблем и статистических данных предложены направления для дальнейшего развития радиолокационного метода наблюдений за метеорами в Казанском федеральном университете. Для повышения точности наблюдений и расширения возможностей метеорного комплекса по регистрации метеорных следов и изучению притока метеорного вещества предлагается увеличить длину измерительных баз до 400 м на 200 м, и также установить дополнительные антенны и приемные комплексы, оснащенные фазовыми интерферометрами, размещенными с значительным пространственным разнесом, а также организовать совместные наблюдения метеорных явлений.

Поступила в редакцию 04.10.2024 г. Принята в печать 14.11.2024 г.

Ключевые слова: метеоры, потоки, метеорный радар, измерительные базы, точность

Prospects for development of meteor radar observations at Kazan Federal University

Korotyshkin D.V., Sherstyukov O.N., Valiullin F.S.

Kazan Federal University, Kazan, Russia

This paper focuses on the modernization of the meteor radar system based on SKiYMET at Kazan Federal University. The goal of this modernization is to enhance the accuracy of radar observations of meteors. As part of the upgrade, the number of antennas was increased from 5 to 12, and the measurement baseline was expanded to 220 meters by 150 meters. These enhancements significantly improved the precision of angular coordinate measurements, achieving accuracies of 0.3 degrees or better. Additionally, the article presents monitoring statistics from 2023, which indicate that the number of recorded meteors with velocity estimates varied between 15,000 and 40,000 per day. Through a detailed analysis of the encountered challenges and statistical data, several directions for the further development of radar meteor observation methods at Kazan Federal University are proposed. To further improve observational accuracy and expand the meteor radar system's capabilities for detecting meteor trails and studying the influx of meteoric matter, it is proposed to increase the measurement baseline to 400 meters by 200 meters. This also includes the installation of additional antennas and receiving systems equipped with phase interferometers positioned with significant spatial separation, as well as the organization of joint observations of meteor phenomena.

Received 04.10.2024. Accepted 14.11.2024.

Keywords: meteors, showers, meteor radar, baselines, accuracy

DOI: 10.51194/INASAN.2024.9.2.006

1. Introduction

The analysis of burning meteors in the Earth's atmosphere provides important data on processes occurring both in our atmosphere and in the solar system as a whole. These studies not only help to investigate the evolution of cosmic bodies, but also reveal the potential risks that meteors may pose to space missions and artificial satellites. This emphasizes the importance of regular and sustained observations of meteor events.

Nevertheless, optical observations encounter challenges: weather factors such as cloud cover and rain, as well as light pollution, make it difficult for astronomers, especially when observations must take place during the morning, daytime or evening hours. An alternative is to use radar observations, which provide a wider and more reliable data set without depending on the time of day. Modern digital advances and solid-state transmitters offer the potential for more regular and in-depth analysis of meteor events, providing the basis for a more comprehensive understanding of these processes and their impact on the Earth and surrounding space.

2. Main problems in radar observations

In this paper we focus on radar observations of meteors. Radio monitoring does not detect the meteor particles themselves, but rather their trails resulting from combustion in the atmosphere. This process is similar to optical methods, where not the particles themselves are observed, but bright flashes associated with the heating and glow of the plasma resulting from collisions of atmospheric molecules with meteoric matter. The trails are ionized

columns of air, several meters in diameter and several kilometers long, formed by the detachment of electrons from air molecules under the influence of high temperatures arising during the combustion of the meteoric body.

Radio monitoring of meteor trails raises several key issues and challenges, among which are statistical availability, accuracy, and noise resistance. These aspects are directly related to meteor radar data, which allow to observe and record meteor trails and to extract the necessary parameters for analysis.

Radio meteor observations fulfill several important tasks. First of all, these are astronomical studies including bolides, meteorites, individual meteors, meteor showers and sporadic sources. The research aims to identify parent bodies such as comets and asteroids and to study their parameters using statistical methods. Meteor velocities, hourly zenith velocity (ZHR), meteor flux, masses, mass distributions, mass indices, and chemical composition are analyzed. Measurements of the angles of arrival of meteor trails allow the determination of the radiant of meteors and meteor showers, which in turn facilitates the extraction of their orbital elements. The main results of such studies have significant theoretical value for understanding the dynamics of the solar system and practical significance in assessing meteor hazards.

The tasks addressed also include meteorological studies, especially the dynamics of the middle atmosphere. Meteor radars provide an opportunity to obtain detailed temporal and spatial characteristics of atmospheric parameters such as zonal and meridional wind speed, temperature and others. Unlike satellite and other remote sensing methods, the radio meteor method has a high spatial and temporal resolution, which makes it possible to study a wide range of atmospheric processes, including seasonal changes in circulation in the upper mesosphere and lower thermosphere, as well as trends in thermodynamic parameters. Wave processes such as planetary waves, tidal motions, internal gravity waves, and mesoscale turbulence are also should be mentioned. All these processed are studied at an altitudinal resolution on the order of 1 km. In recent years, efforts have also been made to study the horizontal spatial structure of wind fields by combining data from several meteor radars, which allows the horizontal structure of dynamical processes to be investigated.

The practical significance of such studies lies in their ability to predict and account for atmospheric dynamics in the context of space launches and meteor aeronomy issues. In addition, the data obtained can be used to create reference models of the atmosphere and for reanalysis of wind parameters.

Different parameters, such as amplitudes and phases of meteor radio reflections, are analyzed as a function of time. In this context, two main approaches are distinguished: continuous wave and pulse. The first approach is easy to implement, but may encounter some problems in signal reception, so in most cases the pulse method is used. This method consists of periodically sending short radio pulses with a certain period related to the pulse repetition frequency (PRF).

The accuracy of various parameters of radio meteor observations depends to a major extent on the power of the radiated signal. However, increasing the power may face both permissive (radio frequency regulation) and hardware limitations. In such circumstances, a strategy of accumulating signals through an increased number of antennas can be used to improve accuracy. For example, this may be applicable for meteor or wind speed determination, and for extracting parameters derived from a meteor radio echo model and empirical data. Increasing the number of antennas improves the accumulation of radio signals, which allows more accurate estimation of signal amplitudes and phases against the background noise, thereby increasing the signal-to-noise ratio without the need to increase the radiated power.

Another important aspect of parameter accuracy is related not only to the number of antennas, but also to their spatial separation. The greater the antenna spacing, the more accurate the parameters, such as the angular and spatial coordinates of the reflection points and meteor burnup regions, can be obtained. This leads to more accurate estimates of the radiant and orbital elements of meteors and meteor showers. However, the extremely large antenna spacing (more than half a wavelength, 0.5λ) creates ambiguities in the estimation of signal path differences, which complicates the determination of arrival angles. For differences between 4.5λ and 7.5λ , the ambiguities can be resolved with additional antennas, and for long bases, the number of antennas must usually increase significantly. This, in turn, leads to an increase in computational cost, which is not a significant problem with the current advances in computing technology.

However, modern radars are equipped with not very powerful transmitters and short baselines (2λ and 2.5λ with a total baseline of 4.5λ). This may be due to spatial constraints encountered when installing meteor complexes at out-of-town radio sites. Thus, these radars do not function as astronomical instruments, but rather as wind profilers. Although some meteors are recorded with highly accurate parameter calculations, the number of such observations is not so large, and it appears that astronomical research is focused mainly on large meteor particles.

Important problem faced by researchers concerns the statistical availability of observations, i.e., the number of registrations per hour, day, and so on. This is related to the number of receiving antennas: a larger number of antennas allows to capture weaker reflections, which, in turn, gives an opportunity to record small and light particles. However, on most radars, the small number of antennas means that the mass region responsible for small particles and meteor dust remains largely unexplored. This is due to the lack of instruments, both optical and radar, to detect them.

Also a problem of radio meteor measurements is that it is not possible to obtain the spatial structure of the dynamics of the middle atmosphere; radars can only determine altitudinal variability. This is due to the fact that radar can determine only radial wind speed based on the Doppler frequency shift. Statistical evaluation assumes homogeneity of the velocity in different directions of observation and the presence of meteor registrations from different azimuthal directions. Attempts to obtain wind speed components (zonal and meridional components) in a certain area often encounter problems with poor conditioning of matrices when using least squares methods.

Based on the analysis of the current state of radio meteor research, several key directions for improving the efficiency and accuracy of measurements can be identified and the following recommendations can be made:

1. Increasing the antenna field and the number of antennas. It is necessary to expand the size of the antenna field and at the same time increase the number of antennas. This will increase the number of recorded weak reflections, including distant or short time reflections, which are characteristic of high altitudes where ambipolar diffusion is high. Significant improvements in the accuracy of estimating the amplitudes and phases of meteor radio echoes will be possible with this approach.
2. Installation of additional radars. It is recommended to install additional radars at a distance of 1–1.5 km, forming long baselines ($100\text{--}150\lambda$). This will make it possible to determine the angular and spatial coordinates of meteor reflections with very high accuracy.
3. Observations from spaced antennas. It is important to make observations of the same meteors, especially of the most powerful reflections, on widely separated antennas. The main radar is already capable of determining the angular and spatial coordinates of the meteor radio echoes, and using a remote station to recalculate the coordinates will allow the wind speeds in the combustion region to be refined for an individual meteor.
4. Installation of passive radars with phase interferometer. The next step is the installation of additional passive radars equipped with a phase interferometer and synchronized with the main radar. These systems will operate on the principle of forward scattering of radio waves and will solve several problems:
 - Eliminating poor matrix conditioning in the least-squares method of determining wind speed, allowing meteors to be observed from different angles.
 - Increase the number of registrations and their accuracy, as radio scattering increases the duration of reflections. If the distance between stations is chosen correctly, the duration can increase by a factor of 2 or more.
 - The ability to observe more high-speed meteors, improving the accuracy of meteor velocity measurements due to oscillations in the amplitude and phase of meteor radio echoes associated with meteors passing through Fresnel zones.
 - Expansion of capabilities of radio meteor complex. Taking into account the high sensitivity of meteor radars to specular conditions, the main radar detects only a part of meteor reflections satisfying these conditions. Some meteor showers may not meet these conditions, but they can still be recorded on an additional remote radar.

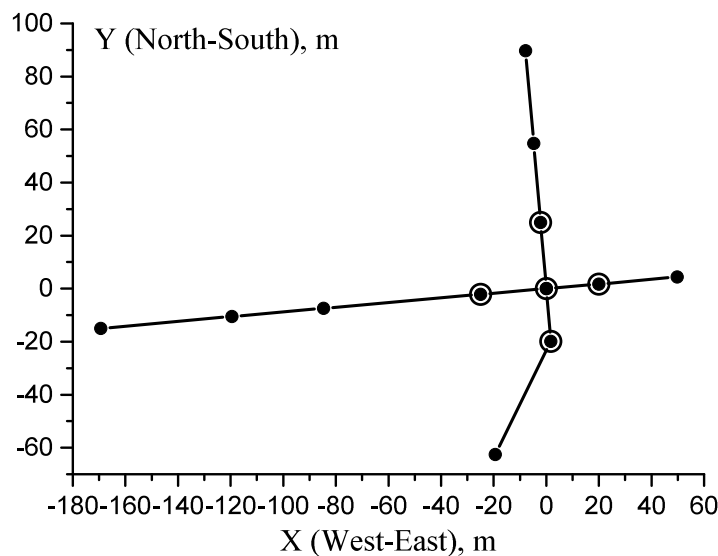


Figure 1: Layout of receiving antennas of the KFU meteor radar (state as of 2024). 5 antennas in the center (points with circles) — initial antenna field in 2015–2020.

3. Meteor radar of Kazan Federal University

Radar observations of meteors in Kazan, Russia, began in 1955 at the Problem Radio Astronomy Laboratory (PRAL) of Kazan University [1]. Regular observations started in 1979 [2], and by 1986 the radar was equipped with a phase interferometer and a 100 kW transmitter [3]. The SKiYMET radar [4] has been operating at Kazan Federal University (KFU) since 2015, and the first results were published in [5].

With the development of digital technologies and computer engineering, a modern radar complex based on the SKiYMET system was created at Kazan Federal University. In 2020, seven additional antennas were installed and twelve superheterodyne receivers with digital data acquisition systems were developed to detect meteor trails.

From 2020 to 2023, experiments were conducted to optimize antenna placement and reduce background noise. The final configuration is shown in Fig. 1, where the unfilled circles represent the original layout and the filled circles represent the current position of the antennas.

The original layout was retained, but additional antennas were added. The non-symmetrical placement of the antennas is due to space constraints and the closeness of buildings, as the science base occupies 260 meters from north to south and 500 meters from west to east, adjacent to a residential area.

The technical characteristics of the meteor radar are presented in Table 1.

Table 1: Featured characteristics of the KFU meteor radar.

Characteristics	Description
1. Radar location	+55.8°N , +48.8°E
2. Method of Probing	Pulsed, backscattered
3. Carrier frequency/pulse repetition frequency	29.75MHz/1594Hz
4. Pulse width	24 μ s
5. Pulse/average transmitter power	15kW/600W
6. Number of transmitting/receiving antennas	1 & 5pcs/12pcs (2015–2020/2020–present)
7. Antenna type: transmit/receive	Crossed Yagi-Udo antennas with 3 and 2 elements. Antennas are All-sky.
8. Overall dimensions of the antenna field	45 \times 45/225 \times 150 meters (2015–2020/2020–present)

Monitoring on the KFU meteor radar is carried out on a 24-hour basis and all year round. During the monitoring meteor radio echoes are detected and recorded in the form of series of amplitudes and phases of radio signals — reflections from meteor trails. The number of such reflections for a day is distributed unevenly, which is associated with the selectivity of the meteor radar. For example, Fig. 2 shows the daily variations of the hourly number of registrations received on 11.02.2023. Its analysis shows that there are time intervals rich in meteor reflections. In other hours, the number of meteors may be small, as can be seen in Fig. 2 from 13 to 18 h local time (+3 h UTC).

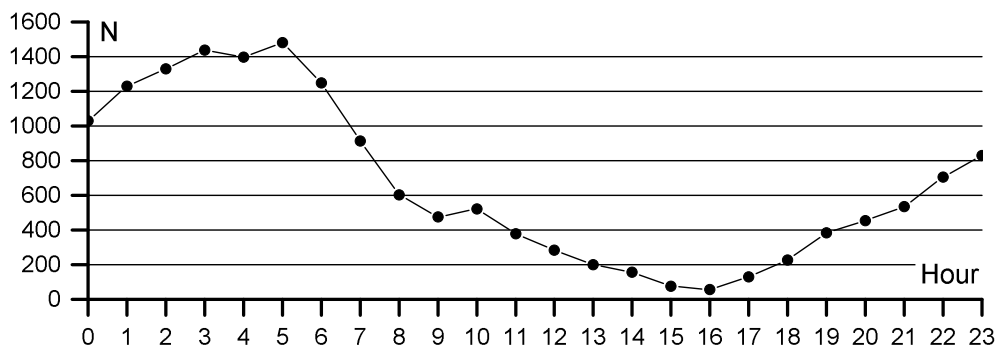


Figure 2: Hourly number of meteor registrations on 11.02.2023 depending on local time (+3UTC).

Another important aspect of radio meteor observations is the seasonal variation in the number of meteor registrations. Fig. 3 shows the seasonal variation in the daily number of meteor registrations. The black line indicates all registrations. We see that the number of meteors recorded by the KFU meteor radar varies from 20,000 meteors per day in February to 60,000 in June-August. This diurnal variation may be related to the selectivity of the registrations of background sporadic sources. The red line indicates the number of meteors with velocity estimates using the [6] method. The number of such registrations ranges from 60% to 70% of the total

number. These registrations are very reliable, since the calculation requires the presence of a meteor signature, i.e., special fluctuations in amplitude and phase associated with Fresnel diffraction. Such meteors per day range from 15,000 at minimum to 40,000 at maximum.

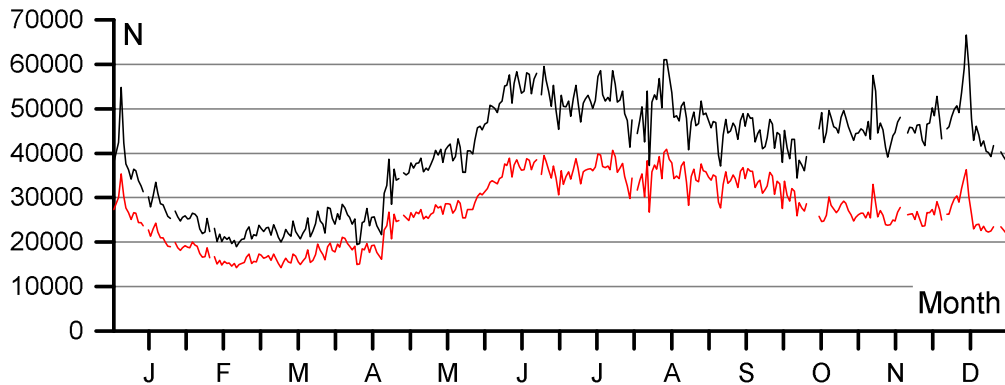


Figure 3: The daily number of meteor registrations in 2023. The black line represents the total number of registrations. The red line shows the number of registrations for which a Fresnel diffraction-based meteor velocity estimate is available.

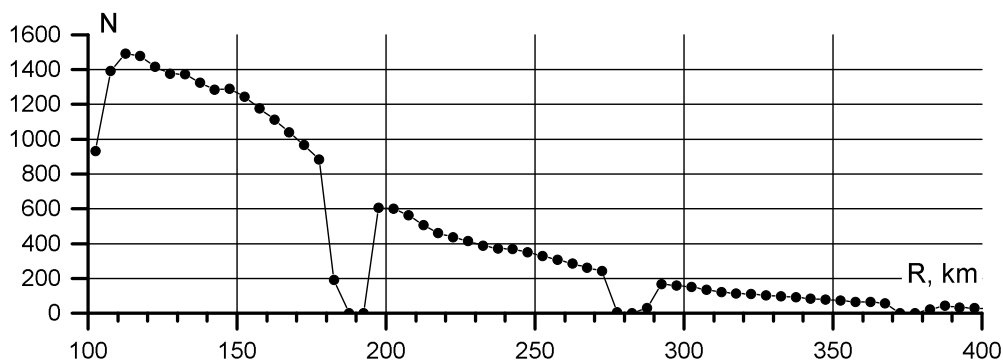


Figure 4: Distribution of ranges averaged over 2023. The number of N is represented at the 5 km interval. Sharp drops are associated with blanking of this range of the direct transmitted pulse.

The KFU meteor radar emits high power radio signals (15 kW in a pulse). Nevertheless, with increasing distance, the signals fade rapidly, and the reflected signals acquired at the receiving antenna have values on the order of $1\text{--}100\ \mu\text{V}$. A very important characteristic of meteor radar is the range distribution (Fig. 4). The figure shows that the number of registrations in the range interval [110–150 km] is approximately the same, and then the number of meteors begins to drop significantly due to the decrease in the power of the reflected signal due to attenuation.

The gaps in the distribution are due to the fact that the pulse repetition frequency (PRF) is 1594 Hz, and the radio wave only manages to travel about 94 km (round trip) during the sounding period, after which a new sounding pulse appears, which masks the meteors with this delay/distance. It is also not possible to record meteors at other ranges, multiples of 94 km, during the sounding period (24 μs).

Meteors burn at altitudes where there is sufficient atmospheric density to heat and ablate the meteor. Radar uses a phase interferometer to determine the arrival angles of the reflected signals, and using the range to the trail, the height of the specular point can be estimated. From the observations in 2023, a distribution of heights is plotted as an annual average. Although this distribution changes slightly during the year, in general the distribution shown in Fig. 5 characterizes the capabilities of the meteor radar: it registers meteor trails in the height range 75–105 km. Outside this range, registrations are possible, but not quite probable.

To accurately determine the angles of arrival of the signals, the differences in the radio wave paths at the different receiving antennas are critical. Therefore, an important aspect is to evaluate the accuracy of meteor radar phase measurements. Fig. 6 shows the distribution of the root mean square (RMS) error σ_Φ of the phase difference Φ at baselines averaged over the year 2023. The errors do not refer to individual meteor radio echo

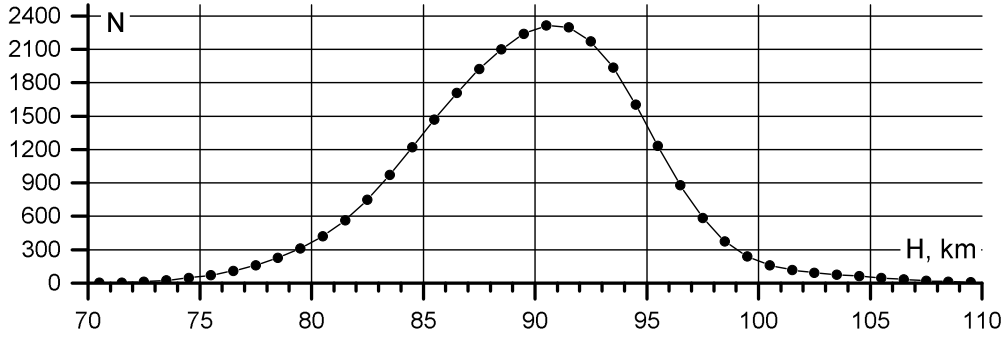


Figure 5: Distribution of heights from measurements on the KFU meteorological radar on average for 2023. N — per 1 km.

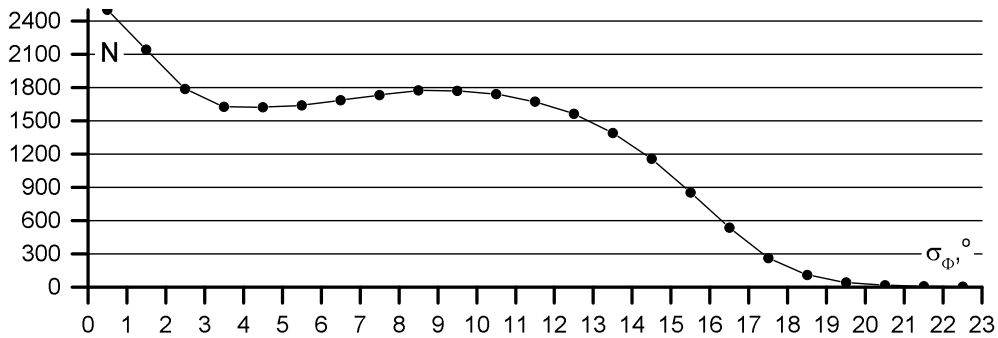


Figure 6: Distribution of RMS errors of phase differences at radar baselines for 01.01.2023–01.01.2024 ($M = 5$). The σ_ϕ step is 1 degree.

pulses, but to the accumulated signal over the entire period of the meteor trail observation. We see that the RMS error of the phase difference is limited to $15 - 20^\circ$.

As an example of meteor radar functioning in monitoring mode, we can present the distribution of the number of shower meteors depending on the day of the year and meteor speed. This distribution was obtained by finding the maximum of the radiant distribution constructed from meteor data using the Jones method [7]. For each construction, samples with a time interval of 1 day and a velocity interval of 10 km/h were used. The obtained results are presented in Fig. 7.

The analysis shows the presence of all major (main) meteor showers and their relative numbers, which characterizes the ability of meteor radar to register reflections from ionized trails left by meteor particles with different velocities and mass distributions. In particular, the number of registrations for Geminids reaches 5800 per day, while for other meteor showers — less than 2 thousand. Small meteor showers are also registered by meteor radar, but are not represented in this diagram because of their small numbers.

4. Further development of meteor radar at KFU

The phase interferometer allows to determine the angles of arrival of radio signals by analyzing the measured phases at the receiving antennas. The phases at the receiving antennas are related to the delay of the received signal relative to the radiated signal due to the path to and from the meteor trail. These data can be considered random. However, the phase difference at two arbitrary baselines is not random; it is related to the wavefront and wave vector (Fig. 8).

In the simplest case, when the antennas are located on the same line, they form an array of measurement baselines with different lengths. The Jones antenna arrangement [8, 9], where the antennas are placed in the form of a cross with different beam lengths (usually 2λ and 2.5λ), is considered to be the classical arrangement. Two perpendicular measuring baselines (maximum in length) are sufficient to determine the angles of arrival. The remaining baselines are used to eliminate the ambiguity of phase measurements. Thus, the angles of arrival can

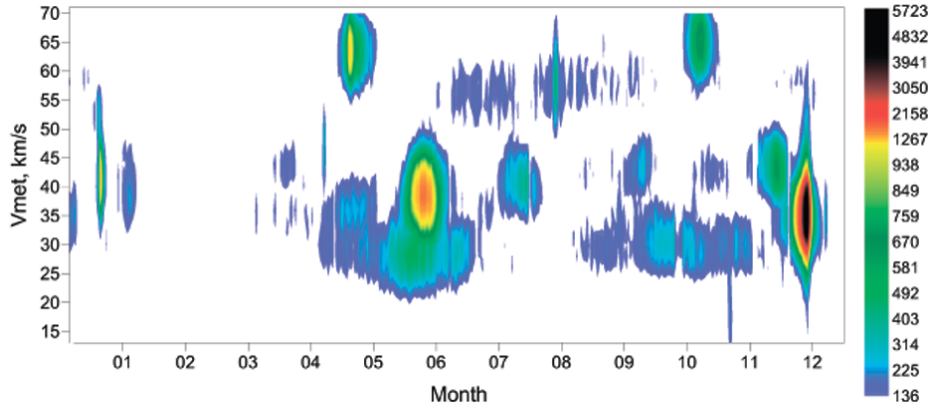


Figure 7: Distribution of the number of stream meteors as a function of day of the year and meteor speed for 2023.

be calculated from the phases at two perpendicular baselines A and B:

$$\begin{cases} \Delta\phi_A = L_A \frac{2\pi}{\lambda} \cos\theta \sin Z, \\ \Delta\phi_B = L_B \frac{2\pi}{\lambda} \sin\theta \sin Z, \end{cases} \quad (1)$$

where θ is the azimuth angle, Z is the zenith angle, L_A and L_B are the lengths of the corresponding baselines in meters, and λ is the wavelength in meters, $\Delta\phi_A$ and $\Delta\phi_B$ are the measured path differences at the baseline.

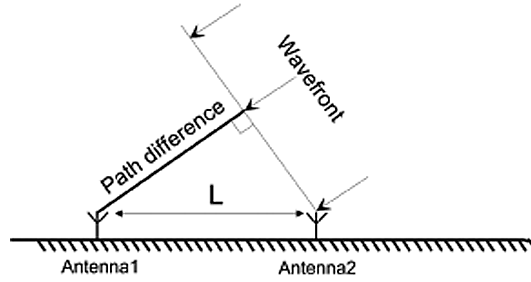


Figure 8: The path difference of the wavefront at the two antennas.

Solving the system of equations (1), we find the values of zenith and azimuth angles. For the trivial case when the azimuthal angle is 0 (as in Fig. 8), we can obtain a single equation, which is easy to analyze:

$$\Delta\phi = L \frac{2\pi}{\lambda} \sin Z. \quad (2)$$

Hence it is easy to obtain that

$$Z = \arcsin\left(\frac{\Delta\phi\lambda}{2\pi L}\right). \quad (3)$$

If we take the derivative of the equation (3) and then apply the expectation operator, we get the variance of the zenith angle estimate as a function of the phase variance at the baseline:

$$D[dZ] = \sigma_Z^2 = \frac{\sigma_\Phi^2}{\cos^2 Z} \left(\frac{\lambda}{2\pi L}\right)^2. \quad (4)$$

Hence the RMS error of the zenith angle can be written as:

$$\sigma_Z = \frac{\sigma_\Phi}{\cos Z} \left(\frac{\lambda}{2\pi L}\right). \quad (5)$$

The formula for the RMS error of the azimuthal angle can be obtained in a similar way, with the only exception that the perpendicular baseline to the azimuthal direction will play a key role here:

$$\sigma_\theta = \frac{\sigma_\Phi}{\sin Z} \left(\frac{\lambda}{2\pi L}\right). \quad (6)$$

In the case where we have multiple baselines, and where the azimuthal angles of arrival are different from 0, the formulas become significantly more complicated, and the RMS error of the estimates will be even better than the estimates obtained by the presented formulas.

Analysis of the formulas (5) and (6) shows that the error of the arrival angles is inversely proportional to the lengths of the corresponding measurement baselines, and also depends on the zenith angle θ . When we receive signals from the zenith ($Z = 0$), we get full uncertainty in azimuth. On the contrary, when we approach a zenith angle of 90° , the uncertainty of the zenith angle increases, while the azimuth angle is measured very accurately.

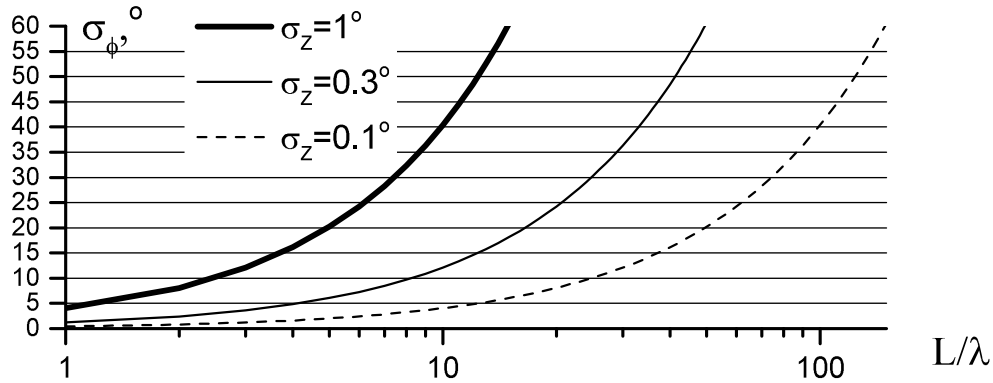


Figure 9: Dependence of the phase error on the baseline length. The graphs are plotted for zenith angle $Z = 50^\circ$.

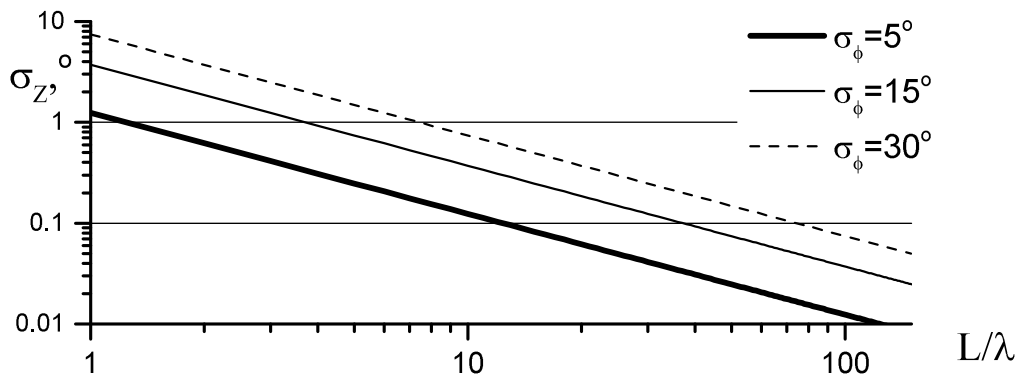


Figure 10: Dependence of the zenith angle error on the baseline length. The graphs are plotted for zenith angle $Z = 50^\circ$.

Using the formula (5), we plot the dependence of the acceptable phase error on the length of the measuring baseline. The graphs are plotted for three cases of interest to us: when the zenith angle error is equal to 1° (coarse case), 0.3° is the median case, and 0.1° is the superior case. Angular resolution better than 0.1° is extremely difficult to achieve due to the fact that long baselines can shift the position of the specular point along the trail from antenna to antenna, which degrades the angular resolution.

Analysis of the plots presented in Fig. 9 shows that an error of 1° is achieved at baselines 4.5λ (SKiYMET layout), and for a number of meteors 0.3° , where a phase error of less than 5° . The current meteor radar antennas layout (Fig. 1) provides a zenith angle accuracy of 0.1° with phase error less than 5° , while the maximum zenith angle error is no worse than 0.3° is obtained for each meteor, since the average phase error is always less than 20° . (see Fig. 6).

Of particular interest are cases when phase estimation is performed not for the whole radio echo, but for a part of it in order to determine the trajectory. In this case, the phase errors are no longer limited at all. Therefore, there is still interest in even longer baselines.

Another approach (Fig. 10) allows us to choose the baseline length based on a fixed phase error (5° , 15° , 30°). The figure shows that, for example, a phase error of 30° (i.e., a variant of phase estimation from a trail fragment) requires a baseline of over 100λ to achieve an angular coordinate error of less than 0.1° .

The proposed (possible) increase of the baseline length, based on a possible cross-shaped layout, up to 400 meters by 200 meters (these are the maximum dimensions of the PRAL radio polygon) at $\sigma_\Phi = 15^\circ$ will allow to obtain errors in zenith angle from 0.09° to 0.18° .

It should be noted that several effects begin to play a role when the baseline length is increased. The first is related to the fact that it will be necessary to take into account the sphericity of the reflected radio wave front, while we assumed its flatness. The second relates to the high accuracy of the antennas setup in the array. The third is that at large baseline lengths there is a strong ambiguity in the phase measurements, which can only be resolved by using an additional array of receiving antennas. Modeling of antenna systems with maximum baseline lengths of 50 by 125λ and an array of 25 antennas, some of which belong to the current antenna arrangement and some of which extend the baselines to the specified sizes, was carried out. Analysis of the simulation results (without taking into account the sphericity effect) showed that the phase ambiguity is completely resolved at the specified antenna layout up to phase errors of 30° . These calculations show that in order to expand the capabilities of the KFU meteor radar, it is quite possible to place additional antennas on the territory of the Engelhardt Astronomical Observatory, which is just located at a distance of 1 km from the radio polygon of PRAL.

5. Radio transmission and reception point separation: meteor forward scattering

In order to receive meteor radar signals at a remote receiving station, it is necessary not only to have receiving equipment, but also to be able to synchronize by carrier frequency and by the beginning of the probing pulse. If the receiving station is within a radius of about 60 km, it is possible to detect a direct signal in the orientation to the meteor radar. For example, measurements with a half-wave dipole antenna at a distance of 45 km from the transmitting antenna of the meteor radar revealed a strong direct signal in the direction to the KFU meteor radar. The signal strength was approximately 7 dB. It should also be noted that the experiment was conducted in a low-lying area where reception degradation can be expected. With coherent accumulation it is possible to significantly increase the signal level in order to more accurately lock the receiving equipment to the carrier frequency and to the beginning of probing by meteor radar.

As it was indicated earlier, to solve a number of meteorological and astronomical tasks, it is useful to install passive meteor radars at a considerable distance from the transmission point. Analysis of Fig. 4 shows that the number of registrations is practically stable for ranges up to 150 km. Considering that the radio wave has to travel twice the distance (in both directions), this value is doubled. The average height $H = 92$ km (Fig. 5) allows us to determine the distance to remote stations, at which the attenuation of radio signals will not be a problem — this distance is up to 240–300 km.

To organize such stations, it will be necessary to install a full-performance phase interferometer including at least five receiving channels (antenna, frequency preselector/amplifier, superheterodyne receiver/SDR receiver). In addition, since it is difficult to expect a direct signal at such a distance due to the lack of line of sight between the receiving and transmitting sites, it is necessary to organize a system of synchronization by the carrier frequency of sounding (for phase synchronization) and the time of the beginning of sounding (for determining the distance to the trail). This can be accomplished using thermostabilized disciplined GPS reference signal generators. Such generators should be used at both the receive and transmit points, collecting calibration information on the exact values of carrier frequency and start of sounding relative to the synchronized GPS generator.

Taking into account that the sizes of antenna fields of remote stations can reach about 100×100 meters, such meteor systems can be installed on the basis of radio polygons of universities located within a radius of 300 km from Kazan.

6. Conclusion

The paper considers the problems arising in radar observations of meteors. The main problem is the small size of the measuring baselines of most modern meteor radars — only 2 and 2.5λ , which leads to total crossed baselines of 4.5λ . There are also a limited number of antennas (5), which limits the application of these radars primarily for meteorological purposes.

The modernized KFU meteor radar has significantly larger measuring baselines (220 m by 150 m) and the number of antennas has been increased to 12 compared to 5 antennas on the classic SKiYMET radar. This improvement allows to increase the accuracy of measurements, achieving a standard deviation of angular coordinates of less than 0.3 degrees, while for SKiYMET this figure is 1 degree. There is also at least a double increase in the number of registrations, from 30,000 to 60,000 during the peak summer months.

As further steps to improve the accuracy of meteor observations, it is proposed to increase the number of receiving antennas and extend the lengths of the baselines to 400×200 meters, refining the current configuration within the existing PRAL area.

Additionally it is proposed to install additional antennas or even phase interferometric systems with significant spatial separation (from several tens to several hundred kilometers). This can be implemented both by radio amateurs and research universities on the basis of radio polygons located in the regions neighboring Tatarstan.

Funding

The work of Korotyshkin D.V. and Valiullin F.S. was funded by a grant from the Ministry of Education and Science of the Russian Federation FZSM-2023-0015, allocated to Kazan Federal University to fulfill a state task in the field of scientific activity.

References

1. K. Kostylev, *Astronomicheskiye osnovy meteornoy radiosvyazi [Astronomical fundamentals of meteor radio communication]* (1970).
2. I. Lysenko, N. Makarov, Y. Portnyagin, B. Kashcheev, V. Lizogub, V. Sidorov, and A. Fahrutdinova, *Journal of Atmospheric and Terrestrial Physics*, **54**, 915, 1992.
3. A. N. Fahrutdinova, V. A. Ganin, N. V. Berdunov, R. A. Ishmuratov, and O. G. Hutorova, *Advances in Space Research*, **20**, 1161, 1997.
4. W. Hocking, B. Fuller, and B. Vandeppeer, *Journal of Atmospheric and Solar-Terrestrial Physics*, **63**, 155, 2001.
5. D. Korotyshkin, E. Merzlyakov, O. Sherstyukov, and F. Valiullin, *Advances in Space Research*, **63**, 2132, 2019.
6. D. Korotyshkin, *Advances in Space Research*, **74**, 4134, 2024.
7. J. Jones and W. Jones, *Monthly Not. Roy. Astron. Soc.*, **367**, 1050, 2006.
8. T. A. Valentic, J. P. Avery, S. K. Avery, and R. C. Livingston, *IEEE Transactions on Geoscience and Remote Sensing*, **35**, 524, 1997.
9. J. Jones, A. R. Webster, and W. K. Hocking, *Radio Science*, **33**, 55, 1998.

О синергии наземных и космических телескопов при обнаружении ОСЗ декаметрового класса в околоземном космическом пространстве

Шугаров А.С., Шустов Б.М.

Институт астрономии РАН, Москва, Россия

Как показало Челябинское событие 15 февраля 2013 г., столкновения малых (декаметровых) тел с Землей могут представлять опасность для жителей нашей планеты. Такие тела малозаметны и могут быть систематически обнаружены только в околоземном космическом пространстве. Необходима всемирная сеть наземных оптических телескопов, позволяющая очень быстро обследовать все ночное небо для обнаружения небольших астероидов в околоземном космическом пространстве. Однако значительная часть объектов, сближающихся с Землей (ОСЗ), приближается к Земле в дневное время, и их можно обнаружить только с помощью специальных космических средств. В предыдущих статьях мы предложили космический проект СОДА (Система обнаружения дневных астероидов), направленный на обнаружение таких ОСЗ на короткой шкале времени (часы). В этой статье мы кратко представляем обновленную информацию о проекте СОДА в сравнении с другими аналогичными космическими проектами. Особое внимание уделяется рассмотрению синергии наземных и космических телескопов для эффективного обнаружения ОСЗ декаметрового класса. Обсуждаются перспективы международного сотрудничества по проекту SODA, в частности, в рамках сотрудничества стран БРИКС в области астрономии.

Поступила в редакцию 09.10.2024 г. Принята в печать 14.11.2024 г.

Ключевые слова: объекты, сближающиеся с Землей (ОСЗ); обнаружение малых ОСЗ; дневные астероиды; проект BITDN; проект СОДА

On the synergy of ground-based and space-born telescopes in the discovery of decameter class asteroids in the near-Earth space

Shugarov A.S., Shustov B.M.

Institute of Astronomy of the RAS, Moscow, Russia

As demonstrated by the Chelyabinsk event on February 15, 2013, collisions of the small (decameter class) near-Earth objects (NEOs) with the Earth can pose a threat to the inhabitants of our planet. Such bodies are faint and can be systematically detected only in near-Earth space. A world-wide network of ground-based instruments is needed, allowing quick survey of the entire night sky to detect small asteroids in near-Earth space. However, a significant portion of NEOs approach the Earth from the day-time sky and they can only be detected with special space-based facilities. In previous papers we suggested the space project SODA (System of Observation of Day-time Asteroids) aimed to detect such NEOs on a short-time scale (hours). In this paper we briefly present updated information about the SODA project in comparison with other similar space projects. Special attention is drawn to considering the synergy of ground-based and space telescopes in exhaustive discovery of decameter class NEOs. The prospects for international cooperation on the SODA project are discussed, in particular, within the framework of the BRICS countries collaboration on astronomy.

Received 09.10.2024. Accepted 14.11.2024.

Keywords: Near-Earth Objects (NEOs); small NEOs detection; day-time asteroids; BITDN project; SODA project

DOI: 10.51194/INASAN.2024.9.2.007

1. On space-born telescopes for observation of asteroids in near-Earth space

Until recently 140 m was considered as the size limit of potentially hazardous NEOs (asteroids and comets), but the Chelyabinsk event on February 15, 2013 clearly demonstrated that decameter class NEOs can be dangerous too. According to the modern paradigm the lower size limit of the potentially hazardous objects has been shifted to 10 m (e.g. NASA's document "National Preparedness Strategy and Action Plan for Near Earth Object Hazards and Planetary Defense"¹). Hence new systems for NEO detection and follow-up should be built in accordance with this new size limit.

Such small NEOs are very faint and can be systematically detected only in near-Earth space. Many projects have been developed with the major task of detecting such potential impactors on night-time sky. To date, most efforts have been focused on ground-based surveys with optical telescopes (see paper by Shustov in this issue). However, a significant portion of NEOs approach the Earth from the day-time sky and they can only be detected with special space facilities.

For further discussion, it is necessary to clarify the concept of the day-time (day-side) sky. The well-known diagram² shows the ratio of fireball phenomena on the night and day part of the sky (Fig. 1). In this diagram the

¹URL: www.whitehouse.gov/wp-content/uploads/2023/04/2023-NSTC-National-Preparedness-Strategy-and-Action-Plan-for-Near-Earth-Object-Hazards-and-Planetary-Defense.pdf — accessed 24.07.2024

²https://www.esa.int/ESA_Multimedia/Images/2016/06/Bolide_airbursts_1994-2013

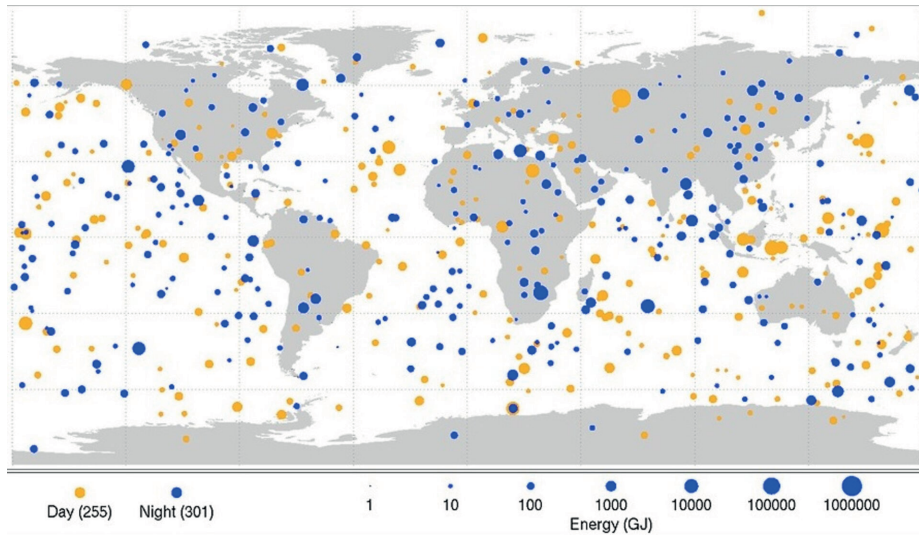


Figure 1: This diagram maps the data gathered from 1994–2013 on small asteroids impacting Earth’s atmosphere to create very bright meteors, commonly referred to as fireball. Sizes of red dots (daytime impacts) and blue dots (night-time impacts) are proportional to the optical radiated energy of impacts measured in billions of Joules (GJ) of energy, and show the location of impacts from objects 1–20 m in size.

daytime sky refers to the part of the celestial hemisphere where the Sun is located, therefore the daytime sky is half of the celestial sphere.

For astronomers, the concept of the daytime sky has a different meaning. This is a part of the celestial sphere on which it is currently impossible to conduct observations with optical telescopes, except for the brightest sources (Sun, Moon, bright planets, etc.). The area of the daytime sky is noticeably smaller than the area of the entire hemisphere.

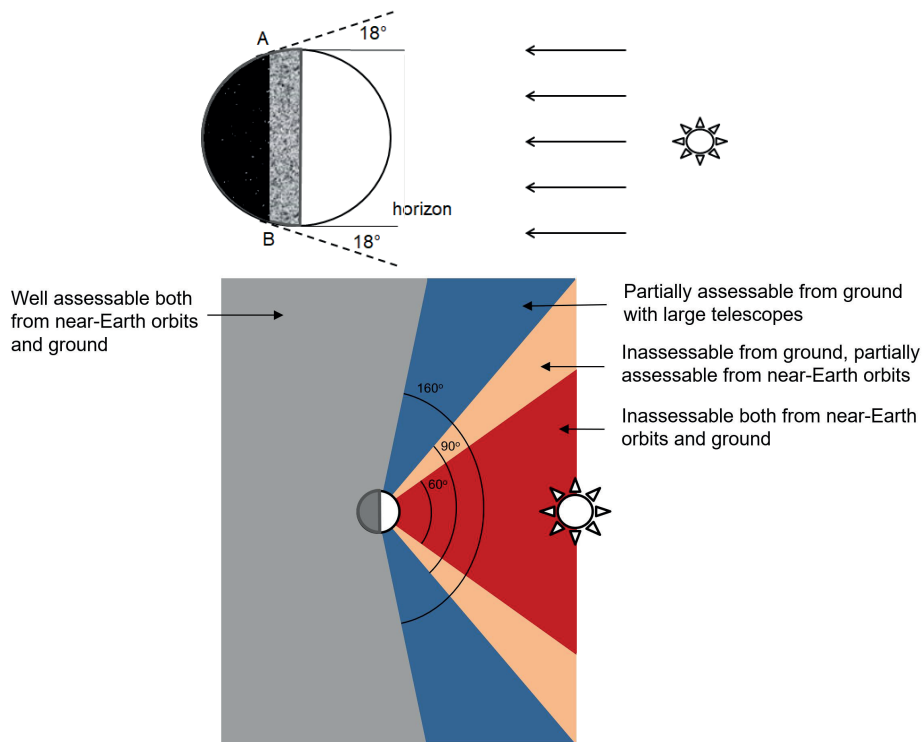


Figure 2: To the concept of the daytime sky during observations with ground-based and space telescopes. Top panel — a theoretical diagram (unrealistic) of the daytime sky during ground observations. Bottom panel — a more realistic diagram of the daytime sky.

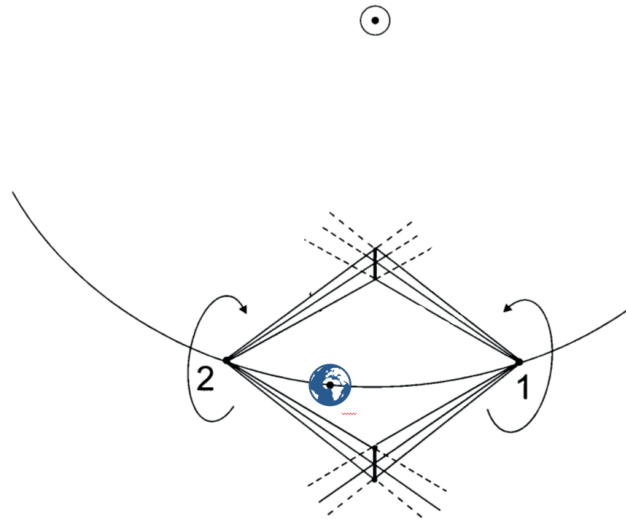


Figure 3: Schematic diagram of telescopes on the Earth orbit (project “Nebosvod” [4]).

Let’s remember that astronomical observations using optical instruments are possible during astronomical twilight, i.e., when the Sun has moved below the horizon at 18° (Fig. 2, top panel). Thus, the inaccessible area for optical observations from the Earth’s surface at a given time theoretically has an opening angle of 36° (18° from the Sun). If observatories were densely and evenly distributed over the globe and especially on the line A–B on the Earth’s surface, it would be possible to observe the entire celestial sphere at a given time, apart from the inaccessible area indicated above. However, this formal analysis does not take into account unfavorable factors such as the uneven distribution of observatories on the Earth’s surface, the fact that far from all of the roughly 1500 observatories (on the International Astronomical Union list) have instruments suitable for this task, and the fact that, on average over the world, the number of observing nights at observatories does not exceed 50% over a year. Another practical factor is that the illumination of the sky in the vicinity of the sunset at the onset of astronomical twilight (up to 20° in elevation from the horizon) hinders accessibility of this area to instruments with the best sensitivity. Our estimates indicate that, when all these factors are taken into account, the daytime sky should correspond to the region around the Sun with an angular radius of no less than 45° . This means that at least 15 percent of the celestial sphere is inaccessible for observations in the optical range from the Earth at any given time. Paper [1] notes that approximately 15.6–19.9% of Earth-threatening NEOs are estimated to be approaching Earth directly from the day side, and are thus very difficult to detect using ground surveys. In practice this percentage seems to be higher.

As it is noted in [2] the regions of the sky within 30° of the Moon or within 15° of the galactic plane are not covered by telescopes due to the increase of the sky background.

Placing a telescope in space does not improve the situation significantly, because the angle of avoidance, e.g. the minimum angle by which the optical axis of the telescope should be turned away from the Sun’s direction, is usually about 30° (Fig. 2, bottom panel).

If observations of asteroids with space-based telescopes are being discussed, then it should be considered that an asteroid located in the near-Earth space at an angular distance of 40° (a phase angle of 140°) from the Sun is only partially illuminated. The same asteroid located at the same distance, but at a phase angle of 40° , is of 1.6^m fainter (see [3]).

The area from 40° to 80° is potentially accessible for ground-based telescopes, but the asteroid detection distance will be highly affected by several factors: unfavorable phase angle, increased zodiacal background, increased Earth atmosphere background close to sunset and sunrise time, possible bad observation conditions close to the horizon. As a result, while it still has a possibility to observe NEOs within 40° to 80° region with large aperture ground telescopes, it can’t be done on a regular basis with typical medium aperture wide-field telescopes (Fig. 2, bottom panel). Therefore, about 40% of the sky is practically unassailable from the ground for regular observations in survey mode with moderate aperture telescopes.

This area around the Sun is subject to survey observations with space born telescopes primarily, while the ground based telescopes may be used for follow-up observations of newly discovered objects.

Space-based surveys offer a clear advantage over ground-based surveys due to their unique possibility to look inside the Earth orbit, and thus monitor those objects coming from the Sun. In section 2 a very brief overview of some space-based projects for NEO detection in near-Earth space is presented.

We have briefly presented updated information on the SODA project in comparison with other similar space projects. In section 3 special attention is drawn to considering the synergy of ground-based and space telescopes in discovery of decameter-class NEOs. Prospects for international cooperation on the SODA project have been discussed too, in particular within the BRICS countries collaboration on astronomy.

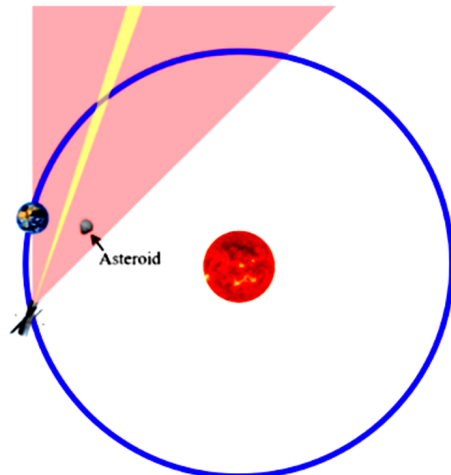


Figure 4: Schematic diagrams of telescopes on the Earth-leading heliocentric orbit. The pink triangle is the visibility zone of the survey telescope and follow-up telescope, and the yellow triangle is the single-visit field of view of the telescope [5].

2. SODA project among other space-based projects for NEO detection in the near-Earth space

In the previous section we argued that space-based surveys offer a clear advantage over ground-based surveys due to their unique possibility to look inside the Earth orbit, and thus monitor those objects coming from the Sun. Space-based systems for detecting hazardous celestial bodies are discussed by experts in various countries. Some of the projects also allow the detection of bodies on the daytime sky. The proposed projects can be divided into two groups according to where the telescope are placed. In the first group there are telescopes placed in the Earth orbit ahead or behind the planet, in the Venus orbit, on the Moon surface, etc. In the second group there are telescopes placed in the vicinity of the L1 point of the Sun-Earth system (SEL1).

In [4] a system of two 1.5 m aperture telescopes is proposed. The telescopes are placed at a considerable distance from the Earth (project “Nebosvod”). The first spacecraft is located ahead of the Earth on the Earth-leading heliocentric orbit (ELHO) at a distance of 0.3 au. The second spacecraft is located behind the Earth on the Earth-trailing heliocentric orbit (ETHO) at a distance of 0.15 au. The system is designed to detect dangerous bodies > 50 m in size. In the main survey mode the telescopes rotate in order that their fields of view form two intersecting cones, where dangerous bodies can be detected (Fig. 3). The system also allows for follow-up observations of known bodies. So far the proposal is in its preliminary stage.

In [5] two telescopes of ~ 1 m aperture were proposed to be deployed on the Earth-leading heliocentric orbit approximately 10 million kilometers ahead of the Earth to detect asteroids approaching the Earth from the sunward direction (Fig. 4). According to authors photometric calculations, from proposed orbit, 1 m aperture telescope can observe > 50 m NEOs close to the Earth with a warning time of several days.

There are suggestions to put the telescope on a Venus-like orbit, at the Moon surface, etc. ([6, 7] and references therein). In our opinion, currently these projects require serious technological advances and have a high cost that may not justify the goal. In addition some of them do not make a breakthrough in detection efficiency of day-time 10 m class asteroids.

Papers [5, 8] provide useful tables with a comparison of the effectiveness of NEO detection by telescopes located in different orbits. We used this idea and somewhat reworked the contents of the table in accordance with what is described in this paper (Table 1). Our major conclusion is that placing a telescope to search for daytime asteroids in the vicinity of SEL1 seems to be the most rational.

In [9, 10, 11, 12] we suggested and described the space system SODA (System of Observation of Daytime Asteroids). SODA is designed to detect nearly all ($> 90\%$) bodies larger than ~ 10 m entering near-Earth space from the day sky.

Table 1: Summary of the advantages and drawbacks of various orbits for space missions aimed at providing early warning for asteroids approaching the Earth from the sunward direction.

Approximate geocentric distance (au)	Orbit type	Main advantages	Main drawbacks	Warning on decameter NEOs in the near-Earth space
10^{-5}	SSO	relatively low cost	poor phase angle, maximal blind zone	no
10^{-4}	MEO, GEO	relatively low cost	poor phase angle, maximal blind zone	practically no
10^{-3}	Moon	serviceable (in future)	less than half-sky accessible at short time scale	too short warning
10^{-2}	Sun-Earth L1 (SEL1)	there is experience in space science	high rate downlink required	reasonable warning (for SODA project)
10^{-1}	ELHO	there is experience in space science, reasonable warning time for both day-time and night-time NEOs	large aperture or IR telescope required, high rate downlink required	warning only > 50 m
10^0	Venus-like	Atiras observable, observation of the whole area inside the Earth orbit	very expensive: large aperture or IR telescope required, high rate downlink is a big problem, several SC needed	warning only for large NEOs

The main idea of the SODA mission is to put one or two spacecraft (SC) equipped with ~ 30 cm aperture wide-field optical telescopes into the vicinity of the SEL1 point to perform observations in a barrier mode (Fig. 5)

A fast slewing pre-aperture flat mirror provides flexible planning of observation strategy for each telescope in a survey mode (barrier detection). It also provides the possibility to track every potentially dangerous object until it approaches the Earth in target mode with very flexible observation parameters.

The estimated number of decameter-size bodies to be detected per year is about 600–1000. This makes it possible to verify current statistical models of minor body population in the Solar system. Smaller meteoroids can be detected with lower completeness.

SODA will be an efficient instrument for the detection of bodies at collision trajectories, especially in the two SC option. SODA is designed to determine the atmospheric entry point with an accuracy of up to a few tens of kilometers and to ensure a 10 hour warning time.

Currently, we are working on the option of one SC. The main advantages of the two SC option in comparison to the one SC option are:

- highly increased accuracy of orbit determination using the triangulation method of observation;
- solution to the problem of missing bodies flying close to the SC (at a distance of less than 0.4 million km);
- increased detection area;
- improved system reliability.

A single SC would be capable alone to reach the main goal of the mission. However because of the missing of some dangerous bodies, the discovery completeness would slightly degrade. In addition, the astrometric accuracy in target mode will also be degraded, which leads to less accuracy of prediction of impact coordinates on the Earth.

In the frame of Russian-Chinese cooperation and BRICS countries collaboration on astronomy we suggest building the second SC similar to the SODA, which would make a significant contribution to solving the problem of 10 m class daytime asteroids detection.

Recently an idea of how to increase the warning time from the SEL1 was put forward by P. Hermosin through private communication. They have suggested to put the telescope at a Forced Stationary Point (FSP) beyond SEL1. This can double or triple the warning time up to 2–3 days in comparison to SEL1, depending on how far the FSP will be from the Earth. The project keep the main advantages of the SEL1 SODA project, such as good visibility conditions for day-time asteroids, high completeness, moderate size telescopes, etc. Mission architecture requires only one SC to be placed at FSP. To maintain the position at FSP, SC needs a constant force against the Sun's gravity (Fig. 6).

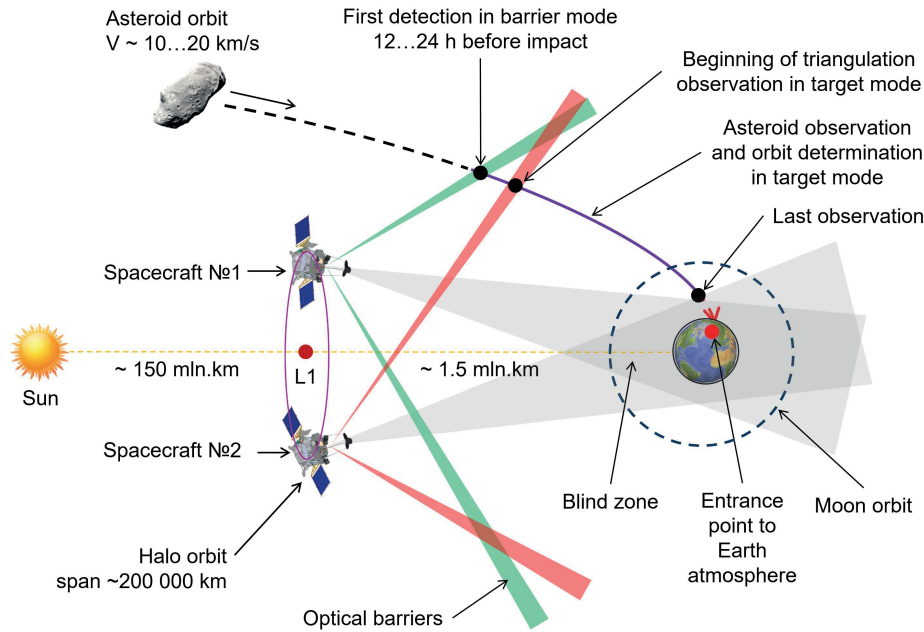


Figure 5: SODA payload scheme of operation from the L1 point of the Sun-Earth system.

Solar sails were suggested to provide the force (see [13]), however they would have to be unrealistically large. The high efficiency ion engine may be used, but they need an unrealistically large amount of fuel. The aperture of the telescope, and, accordingly, its mass, with the same limiting magnitude for detecting decameter bodies, increases with distance from the Earth, which therefore increases the required constant force to keep SC at FSP.

After consideration, taking into account the current technological level, the idea to use FSP is considered as non feasible. Therefore, the SODA project remains the optimal one.

The NEO Surveyor (NASA) project attracts the attention of many researchers since this powerful observatory is scheduled for launch in 2027. The mission is designed to discover and characterize near-Earth asteroids and comets [14, 15]. The mission's primary objective is to find the majority of objects large enough to cause severe regional impact damage (> 140 m) within its five-year baseline survey. Operating at the Sun-Earth L1 Lagrange point, the IR telescope will survey from 45 degrees to 120 degrees of the Sun.

The survey cadence is optimized to provide observational arcs long enough to reliably distinguish near-Earth objects from distant asteroids that cannot pose an impact threat. A given region of sky is reobserved every 13 days, as long as it remains within the solar latitude-longitude constraints. Over the course of its survey, the NEO Surveyor is expected to discover $\sim 200\,000$ – $300\,000$ new NEOs down to sizes as small as ~ 10 m (but in fact only a small share of them) and thousands of comets, significantly improving our understanding of the probability of an Earth impact over the next century.

The main scientific idea of the NEO Surveyor is from SEL1 its IR telescope will be able to observe the Main asteroid belt well and further beyond it. This will speed up the cataloguing process of all large (> 140 m, partially > 50 m) bodies of the Solar system. It was demonstrated that when a very large ground-based telescope (e.g. LSST) and space telescope at SEL1 work together, the cataloguing rate will double.

This is a completely different approach compared to SODA. SODA catches small 10 m class asteroids directly near the Earth, which cannot be catalogued in any other way, as they are too small and they appear in the near-Earth space for a very short time (a few days at maximum).

These two approaches — cataloguing large bodies (> 50 m or > 140 m) to make a long term prediction and discovering small bodies (> 10 m) in close proximity to the Earth complement each other well. We may state, that NEO Surveyor and SODA space missions at SEL1 complement each other, and they are not competitors.

The cost of the NEO Surveyor mission is about 1 billion USD. The cost of the SODA project is expected to be up to 5 times cheaper, while the project still keeps very significant scientific and practical outcomes for the asteroid hazardous problem concerning day-time asteroids.

3. On the synergy between ground-based and space-born telescopes

A combination of SODA and ground-based survey telescopes (e.g. SiTian, BITDN, ATLAS, etc.) is a way to provide an efficient all-sky system for the detection of decameter size NEOs.

SEL1 is an appropriate point to observe NEOs coming from the Sun, because of an optimal phase angle and absence of background. Ground base system efficiency is remarkably affected by weather, observation conditions and a specific aspect of day-time NEO observations — the phase angle. To be competitive with the SODA project in terms of NEO detection efficiency, one needs a distributed network of optical survey telescopes with a limiting magnitude of about 19^m , which corresponds to a telescope aperture of about 0.5 m and a resulting all-sky survey cadence time of about 1 h.

The combined detection zone of 10 m bodies with a ground-based telescope (19^m limited mag.) and SODA (17^m limited mag.) is shown in Fig. 7. The SNR is shown by color isophotes (green and blue) in 3 unit increments. Blue and pink dotted curves show $SNR = 9$ (quite reliable detection) for ground-based and SODA telescopes respectively.

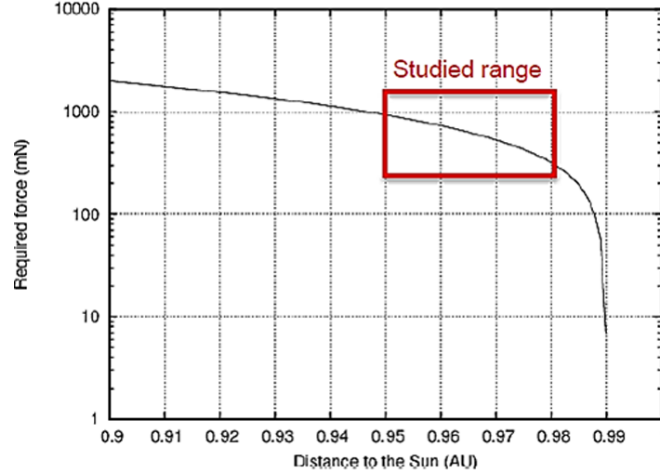


Figure 6: The required force for 1 ton SC to maintain position at a given distance from the Sun.

The plot demonstrates that objects approaching the Earth along the Earth orbit have the shortest detecting distance (0.5 million km) and therefore the shortest warning time. These objects are difficult to observe with ground base telescopes because of the unfavorable phase angle and necessity to observe close to the horizon. For the SODA project these objects are also difficult to observe, because 1.5...2 million km is close to the 30 cm telescope detection distance limit for 10 m size NEOs.

In the frame of BRICS countries collaboration on astronomy it was suggested to build BRICS Intelligent Telescope and Data Network (BITDN) [16]. This ambitious project has a goal to build a network of 1 m class optical telescopes with the unprecedented ability to observe the entire sky continuously on a timescale of less than an hour. BITDN will greatly increase our ability to detect and study asteroids, transient and time-variable phenomena in the Universe, etc. Thanks to the BRICS countries unique worldwide geographical distribution, the future BITDN network may completely solve the problem of 10 m class NEO detection on the night-time sky with a warning time of up to several days.

China has begun a very ambition national project SiTian with the goal to get an entire sky image every 30 minutes in 3 photometrical bands [17]. It is planned to build about 70 telescopes with 1 m aperture and 5×5 deg field of view mosaic detector (18×18 k pixels), the first telescope has already been built. After deployment, a full-scale SiTian project will contribute a lot to NEO detection in the near Earth space at a distance of up to several million km from the Earth.

Collaboration between SODA and other ground based facilities, including telescopes with spectroscopic capabilities, are needed for NEO characterisation.

SODA cooperation with ground-based radio radars for rapid follow-up observation may help improve the accuracy of dangerous bodies orbit determination and provide independent confirmation concerning the threat of impact on the Earth.

4. Conclusions and prospects

The Chelyabinsk event changed our view on the asteroid and comet hazard problem. We understand that it is necessary to build special facilities to detect decameter size bodies coming from the day-time sky.

10 hours of warning time provided by SODA project is sufficient to decrease consequences of asteroid impacts. A larger warning time is possible, but would significantly increase the cost and complexity of the mission.

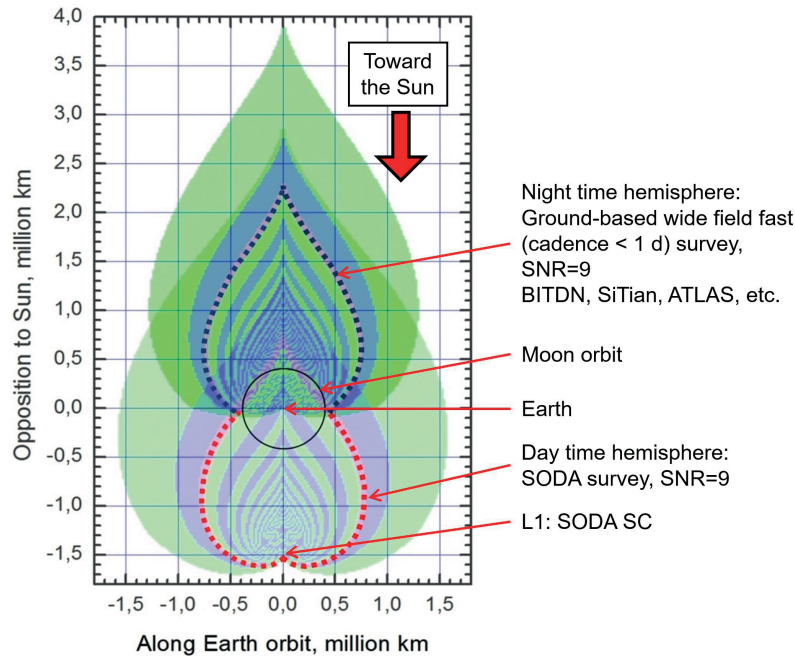


Figure 7: SODA and ground-based telescopes joint operation visibility zone.

It is planned to build one SODA spacecraft as part of the Russian national space safety program “Milky Way”. International collaboration with China and BRICS countries are welcome to build the second spacecraft to improve efficiency and redundancy of the system. We believe that the combination of space-based (SODA) and ground-based (e.g. SiTian, BITDN, etc.) projects is a proper way to build an efficient and realistic warning system against small decameter size impactors.

References

1. O. Ramirez Torralba, R. Jehn, D. Koschny, M. Frühauf, L. S. Jehn, and A. Praus, *arXiv e-prints*, arXiv:1903.08413, 2019.
2. D. Farnocchia, F. Bernardi, and G. B. Valsecchi, *Icarus*, **219**, 41, 2012.
3. C. W. Allen, *Astrophysical Quantities*, London: Athlone (3rd edition) (1976).
4. V. A. Emelyanov and Y. K. Merkushev, in *Protecting the Earth against Collisions with Asteroids and Comet Nuclei*, 369 (2010).
5. X. Wang, J. Zheng, M. Li, H. Zhao, and Y. Wang, *Icarus*, **377**, 114906, 2022.
6. X. Zhou, X. Li, Z. Huo, L. Meng, and J. Huang, *Space: Science and Technology*, **2022**, 9864937, 2022.
7. N. Myhrvold, *Publ. Astron. Soc. Pacif.*, **128**, 045004, 2016.
8. E. Perozzi, M. Ceccaroni, G. B. Valsecchi, and A. Rossi, *European Physical Journal Plus*, **132**, 367, 2017.
9. B. M. Shustov, A. S. Shugarov, S. A. Naroenkov, and M. E. Prokhorov, *Astronomy Reports*, **59**, 983, 2015.
10. A. Shugarov, B. Shustov, and S. Naroenkov, *Open Astronomy*, **27**, 132, 2018.
11. B. Shustov, A. Shugarov, S. Naroenkov, and I. Kovalenko, in *1st NEO and Debris Detection Conference-ESA2019*, 50 (2019).
12. A. S. Shugarov and B. M. Shustov, *INASAN Science Reports*, **7**, 85, 2022.
13. A. F. Mora and J. Heiligers, *Journal of Guidance Control Dynamics*, **43**, 1740, 2020.
14. A. K. Mainzer, J. R. Masiero, P. A. Abell, J. M. Bauer, et al., *Planetary Science Journal*, **4**, 224, 2023.
15. O. Lay, J. Masiero, T. Grav, A. Mainzer, F. Masci, and E. Wright, *Planetary Science Journal*, **5**, 149, 2024.
16. D. Buckley, in *3rd Annual Conference of the African Astronomical Society (AfAS-2023)*, 21 (2023).
17. J. Liu, R. Soria, X.-F. Wu, H. Wu, and Z. Shang, *Anais da Academia Brasileira de Ciencias*, **93**, 20200628, 2021.

Малые тела Солнечной системы: научные и практические вопросы проекта BITDN

Шустов Б.М.

Институт астрономии РАН, Москва, Россия

Тема малых тел Солнечной системы — это гигантская область научных исследований. Малые тела несут информацию обо всех уголках Солнечной системы. Важно, что многие фундаментальные исследования малых тел имеют очень тесную связь с практическими вопросами нашей жизни. В частности, происхождение и эволюция популяции ОСЗ (объектов, сближающихся с Землей) тесно связаны с проблемой астероидно-кометной опасности. Ранее в проекте OTN (Optical Transient Network) [1], получившего затем название BITDN (BRICS Intelligent Telescope and Data Network), предлагалось создать сеть из нескольких широкоугольных телескопов 1-метрового класса и включить в список задач сети помимо наблюдений транзитных астрофизических явлений также и тематику ОСЗ. В данной работе анализируются перспективы инструментов для наблюдений ОСЗ и делается вывод, что наряду с 1-м телескопами необходима широкая сеть малоапертурных инструментов, позволяющих очень быстро (за часы) провести обзор всего неба для обнаружения малых (декаметровых) астероидов в околоземном пространстве. Предлагается мультиапертурный вариант такого инструмента.

Поступила в редакцию 03.10.2024 г. Принята в печать 18.10.2024 г.

Ключевые слова: малые тела Солнечной системы, астероидно-кометная опасность, сотрудничество БРИКС по астрономии, проект BITDN

Small bodies of the Solar system: scientific and practical issues of the BITDN

Shustov B.M.

Institute of Astronomy of the RAS, Moscow, Russia

The topic of the Solar System small bodies (SSSB) is a gigantic field of scientific research. Small bodies carry information about all corners of the Solar system. It is important that many fundamental studies of small bodies have significant connections with the practical issues of our lives. In particular, the origin and evolution of the population of NEOs (near-Earth objects) are closely related to the problem of asteroid-comet hazard. Earlier, the OTN (Optical Transient Network) project [1], now called BITDN (BRICS Intelligent Telescope and Data Network), proposed to create a network of several 1-meter wide-angle telescopes and include in the list of network tasks, in addition to observations of transient astrophysical phenomena, also the subject of NEOs. In this paper, the prospects of instruments for observing NEOs are analyzed and it is concluded that, along with 1-m telescopes, a wide network of low-aperture instruments is needed, allowing very quickly (in hours) to survey the entire sky and detect small (decameter) asteroids in the near-Earth space. A multi-aperture version of such a telescope is proposed.

Received 03.10.2024. Accepted 18.10.2024.

Keywords: small bodies of the Solar system, asteroid-comet hazard, BRICS astronomy cooperation, BITDN project

DOI: 10.51194/INASAN.2024.9.2.008

1. Introduction

Let's recall the basic definitions. According to the Resolution B5 of the General Assembly of the IAU the Solar system small bodies (SSSB) are objects that by their characteristics cannot be attributed either to dwarf planets or to planets or their moons. It is explained by the Resolution that this group includes most of the asteroids of the Solar system, most of the trans-Neptunian objects, comets and other bodies. Meteoroids and interplanetary dust also belong to big class of the small bodies of the Solar system. Until recently, there was no clear criterion for separating the concepts of "asteroid", "meteoroid" and "interplanetary dust". In 2017 the IAU F1 Commission adopted recommendations on the use of the terms "meteoroid" and "interplanetary dust", allowing for a unambiguous use of these terms. According to these recommendations:

- meteoroids — interplanetary solid objects ranging in size from about 30 microns to 1 m;
- interplanetary dust — solid interplanetary objects up to 30 microns in size.

It follows from these definitions that asteroids (and comet nuclei) are solids larger than 1 m.

The topic of SSSB is a vast field of scientific research. As it was noted in Planetary Science and Astrobiology Decadal Survey 2023–2032¹ "small bodies are time-capsules of different eras of Solar system history from the most primitive materials within the Solar system to evolved pieces of larger bodies". Small bodies carry information about all corners of the Solar system.

It is important that many fundamental studies of small bodies have significant connections with the practical issues of our lives. The most important connections are:

¹<https://www.nationalacademies.org/our-work/planetary-science-and-astrobiology-decadal-survey-2023-2032>

Table 1: Dependence of the completeness of NEO detection on the NEO size.

NEO size, m	10	50	140	1000	10 000
Completeness of detection, %	~ 0.03	~ 7	~ 40	> 95	100
Practically possible lead time	hours — few days	years	years	many years	many years

- The origin and evolution of the NEO (Near Earth objects) population is closely related to the problem of asteroid-comet hazard and to the issue of planetary resources.
- Meteoroidal environment is closely related to the problem of safety of space activities (especially in the near-Earth space).

The project BITDN (BRICS Intelligent Telescope and Data Network) is expected to provide a significant contribution to solving the NEO problem. In section 2 a brief analysis of the use of telescopes for NEO detection is carried out and it is shown that at present the problem of detecting small objects is the most urgent and the existing means are not effective enough. A wide-world network of low-aperture instruments is needed, allowing very quickly (in hours) to survey the entire sky and to detect small (decameter) asteroids in near-Earth space. In section 3 it is proposed to include the issue in the BITDN list of tasks. A variant of the ultra-wide-angle multi-aperture telescope system under construction at INASAN, which could enter the BITDN network, is described.

2. NEOs as a target for the BITDN

A near-Earth object (NEO) is asteroid or comet orbiting the Sun with perihelion distance less than 1.3 au. If an NEO's orbit approaches the Earth's orbit at distance less than 0.05 au, and the object is larger than 140 meters across, it is considered as a potentially hazardous object (PHO). PHOs are subset of NEOs. Most known NEOs are asteroids, but about 0.35% are comets.

Until recently 140 m was considered as a “standard lower limit of the size of PHO” but the Chelyabinsk event in 2013 showed that decameter bodies can be dangerous too. Moreover, on a short time scale (hundreds of years) they are even more dangerous than larger bodies because they collide with the Earth much more often. According to the modern paradigm the lower limit of the size of PHO has been shifted to 10 m. Hence a system for NEO detection and monitoring should be built in accordance with this new limit.

The major practical issues of the NEO problem are:

1. Detection and characterisation of all dangerous bodies.
2. Risk assessment in a case of a specific collision threat.
3. Countering and mitigation (reducing damage).

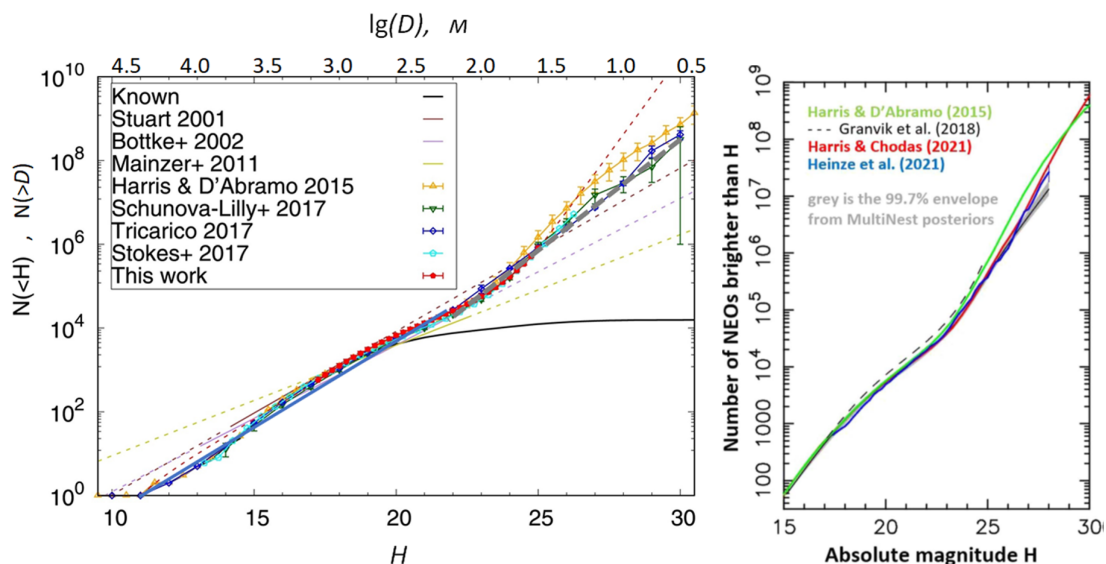


Figure 1: Left panel: the observed cumulative distribution of NEOs on H (also on diameter D) according to the model [2] (marked as “this work”) and models presented in the works of other authors. Right panel: similar distributions from the modified model (solid black line) [3]. Distributions presented in papers by the other authors are presented too.

The first problem and a significant part of the second problem is the field of responsibility of astronomers. Obviously the first problem is of the highest priority. Solving the task means that the following questions will be answered: how many of NEOs (particularly PHOs) do exist in the Solar system? What are their properties? How to find them?

The answers can only be obtained if an efficient global system for detecting and monitoring potentially hazardous space object will be created. At the moment such a system does not exist although the progress made in recent years is impressive. Let's look at this issue in a little more detail.

Completeness of NEO detection permanently increases and it is commonly believed that to date a detection completeness for bodies larger than ~ 1 km (more accurate 0.7 km) has been achieved at the level of $\sim 90 - 95\%$. However as it was mentioned above the current view at NEO problem relates to collisions with bodies ranging in size from decameter (to half a kilometer). Larger bodies collide with the Earth so rarely that these events have no practical interest. For smaller NEOs the completeness of detection decreases significantly with a decrease in the size. This is illustrated in Table 1, based on estimates from the NASA's document "National Preparedness Strategy and Action Plan for Near Earth Object Hazards and Planetary Defense"².

The colors of the cells in the last row in the Table 1 have been added to highlight the level of our awareness. Almost all the largest bodies (over 1 km in size, green cell) are quite confidently tracked by modern means and no additional efforts (programs) are required to find them. Moreover, the time of approach of such NEOs is large and it is quite sufficient to reveal the various characteristics of the NEOs. Medium-sized bodies (over 50 m, yellow cell) obviously require increased attention. The completeness of their detection is insufficient. It is necessary to further develop means of detecting and monitoring them. As to the decameter bodies (over 10 m, red cell) we can state our unpreparedness for, since lead time for such bodies is short. Moreover, as it will be noted later, substantial share of them approach the Earth from the side of the daytime sky. Here, the available detection tools are completely insufficient and it is urgently necessary to develop appropriate programs.

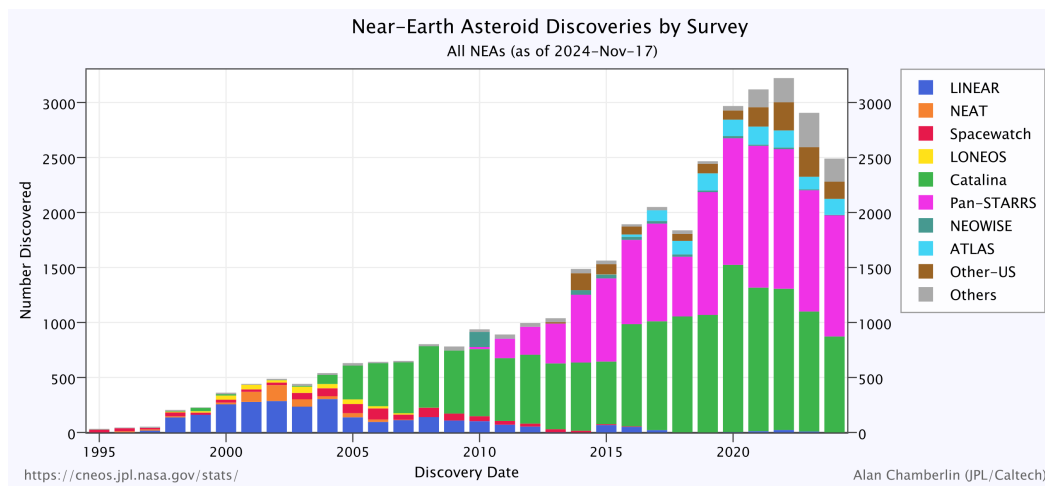


Figure 2: Annually discovered NEAs by survey since 1995. Courtesy NASA/JPL-Caltech.

The incompleteness of the observational data implies the use of various models to describe the NEO size spectrum. Models give a very large spread of the number of bodies of a given size, the smaller bodies, the greater spread. Fig. 1 represents cumulative distribution of known NEOs by absolute asteroid stellar magnitude H (also by diameter D). The left panel is drawn according to the model [2] (marked as "this work") and models presented in the works of other authors. Similar distributions based on more recent data and model NEOMOD (see [3]) are presented at right panel of Fig. 1.

Identification of the size spectrum of small asteroids remains a serious scientific challenge. As it is seen from Fig. 1 the spread of estimates of the number of 10 m bodies reaches two orders of magnitude on the left panel and about one order of magnitude on the right panel. Obviously, the statistics of decameter NEOs needs to be improved and this can only be done by observations. This should be taken into account in observation programs.

As practice shows an universal instrument (telescope) for the timely detection of NEOs of all sizes (from 10 m and above) is hardly to be created. Neither relatively big telescopes (like most productive Pan-STARRS³, Catalina

²<https://www.whitehouse.gov/wp-content/uploads/2023/04/2023-NSTC-National-Preparedness-Strategy-and-Action-Plan-for-Near-Earth-Object-Hazards-and-Planetary-Defense.pdf>

³<https://outerspace.stsci.edu/display/PANSTARRS/>

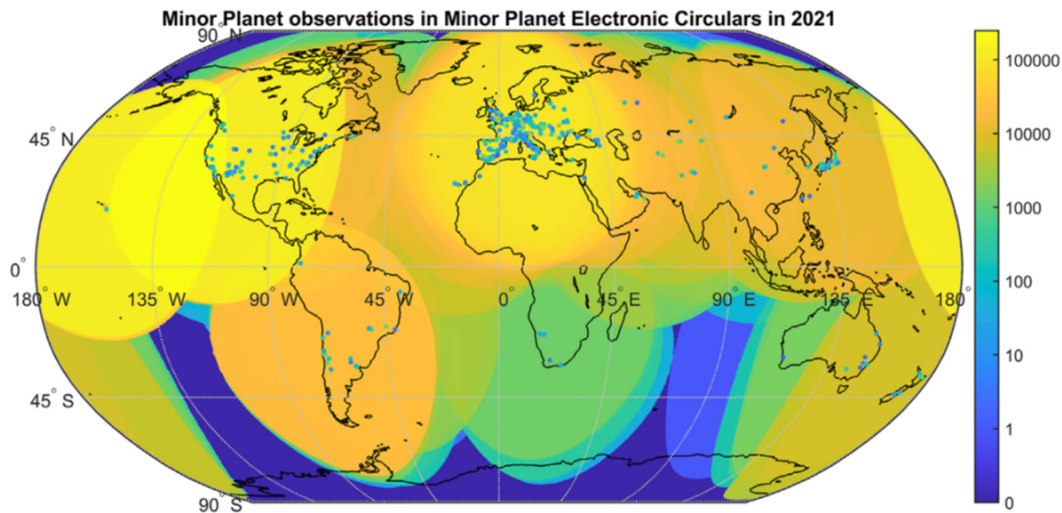


Figure 3: Number of observations published in the Minor Planet Electronic Circulars (MPECs) in 2021. The individual MPC observatories are mapped as points on their geographic coordinates with their number of observations as color. Observatories with no observations in 2021 are removed. The cumulated observations within an arc of 45° of the geographic coordinates is contoured [8].

Sky Survey (CSS)⁴ and ZTF⁵), nor promising “Fly eye” telescope NEOSTEL [4], nor coming soon huge ($\omega = 3^\circ$, $\varnothing 8\text{ m}$) telescope LSST [5], nor the space infrared observatory NEO Surveyor [6] is a panacea. These instruments are not designed for very quick all-sky surveys mode which is required if you try to detect decameter class bodies.

In [7] necessity of two-mode structure for building ground-based system for NEO detection is argued. These two modes are:

Long-range detection mode (NEO size $> \sim 50\text{ m}$, see yellow cell in Table 1).

- Lead time ~ 30 days.
- Time for all-sky survey (cadence) $< \sim 5$ days.
- It is necessary to work at the limit of 23^{m} V , which requires for wide-angle ($\omega > 1^\circ$) large-aperture ($\varnothing \sim 1\text{ m}$) telescopes.

Short-range detection mode (NEO size $> \sim 10\text{ m}$, see red cell in Table 1).

- Lead time ~ 1 day.
- The time for all-sky survey — few hours.
- Extended network of wide-angle ($\omega > 4^\circ$) small-aperture ($\varnothing < \sim 0.5\text{ m}$) telescopes of the visible range is required. It is necessary to work at the limit of 17^{m} V .

All the large telescopes mentioned above work in the long-range detection mode. There exists network Asteroid Terrestrial-impact Last Alert System (ATLAS) that works in short-range detection mode too. As it is presented at home page of ATLAS⁶ the full ATLAS concept consists of eight 50-centimeter diameter $f/2$ Wright-Schmidt telescopes, spread over the globe for full-night-sky coverage. The current system consists of four such telescopes: two telescopes operate in the Hawaiian Islands, the third telescope is at the South African Astronomical Observatory and the fourth in Chile. This system can image the whole night sky visible from a single location with about 1000 separate telescope pointings. At 30 seconds per exposure plus 10 seconds for simultaneously reading out the camera and repointing the telescope, each ATLAS unit can therefore scan the whole visible sky a little over once each night, with a median completeness limit at apparent magnitude 19. Each telescope actually observes one quarter of the sky four times in a night at approximately 15-minute intervals. The four exposures by a telescope allow to automatically link multiple observations of an asteroid into a preliminary orbit, and to predict its approximate position on subsequent nights for follow-up. Pan-STARRS goes approximately 100 times deeper, but needs weeks to scan the whole sky just once. This makes ATLAS better suited to finding small asteroids which can only be seen during the just few days that they brighten dramatically when they happen to pass very close to the Earth.

Relative input of the telescopes in the discovery of NEAs is illustrated in Fig. 2 taken from JPL CNEOS site (https://cneos.jpl.nasa.gov/stats/site_all.html).

⁴<https://catalina.lpl.arizona.edu/>

⁵<https://www.ztf.caltech.edu/>

⁶<https://atlas.fallingstar.com/index.php>

Parameter (8x telescope)	Value
Detector of single tube	CMOS GSENSE6060 BSI 6k x 6k 10 μ m pixel
Pixel format	12k x 24k
Number of pixels, Mpixel	298
Pixel scale, arcsec/pix	5.2
FoV, deg	17.6 x 35.2 *
FoV, sq. deg	574
Readout time, s	< 1
All-sky (20000 sq.deg) survey time** and limiting magnitude at best conditions	
All-sky @ 10 s exposure	10 min @ 18.3 ^m
All-sky @ 30 s exposure	20 min @ 18.9 ^m
All-sky @ 100 s exposure	1 h @ 19.4 ^m

* Fill factor=92%

** Repointing time 5 s



8x VT-78d on
ASA DDM160 mount

Figure 4: General view and technical characteristics of INF [10].

ATLAS is a good example of a system operating in both modes (long-range and short-range ones) although it is not as effective in long-range detection as Pan-STARRS. But it requires as any optical telescope for perfect weather conditions. The four telescopes together can observe the full night sky every night, but bad weather at one or the other site, occasional technical problems, and other factors reduce the effective coverage rate.

Trying to guarantee continuous sky coverage our Chinese colleagues work on an ambitious project SiTian [9]. SiTian is a ground-based all-sky optical monitoring project, developed by the Chinese Academy of Sciences. The concept is an integrated network of dozens nodes of 1-m-class telescopes deployed partly in China and partly at various other sites around the world. SiTian will scan at least 10 000 square degrees of sky every 30 min, down to a detection limit of $V \sim 21^m$. The plan is to complete the installation of 72 telescopes by 2030 and start full scientific operations in 2032.

As it was mentioned in [1] small-aperture systems (e.g. Evryscope⁷, SuperWASP⁸, GWAC⁹) can survey the whole sky very quickly (up to few tens of minutes), but they are unable to provide sensitivity sufficient to detect 10-m class objects at distances greater than a 1 million kilometers.

So far, most of the detections of dangerous celestial objects are carried out not by means of the BRICS countries as it is seen from Fig. 3 (see also Fig. 2). Obviously, the contribution of BRICS countries is still relatively small and needs to be increased.

3. On the BRICS network for NEO observations

The BRICS Astronomy Working Group (BAWG) initiated the project “BRICS Intelligent Telescope and Data Network (BITDN)”¹⁰ (former name — “BRICS Optical Transient Network” (BRICS OTN)). This is a dedicated BRICS-wide flagship program to develop a network of 1 m ground-based optical telescopes for an all-sky survey to detect short lived optical transients and to allow follow-up of multi-wavelength and multi-messenger transient objects (see [1]).

As to the NEO topics an ideal BITDN is expected to meet the goal for successful detection and orbit determination of NEOs down to 10 of meters in size over the full sky every few hours, reaching a limiting magnitude 20^m. The survey observation strategy should to allow for dedicated follow-up of PHO alerts, allowing to track the path of the incoming object and compute the most likely location of impact.

As it follows from the discussion in the previous section, the main problem of NEO detection is the detection of small (decameter) bodies entering near-Earth space at very short time scale. To accomplish this task, the proposed network of four 1 m aperture telescopes seems insufficient, although its contribution to the detection of larger objects in the long-range detection mode is expected to be significant.

Even a future network of telescopes SiTian is unlikely to be able to complete this task in full unless the network nodes are distributed around the globe. After all, most of the nodes will be located within China. In

⁷<https://evryscope.astro.unc.edu/>

⁸<https://www.superwasp.org/>

⁹<https://www.svom.eu/en/gwac-ground-wide-angle-telescope-en/>

¹⁰<https://www.bricsastronomy.org/brics-intelligent-telescope-and-data-network/> — accessed 28.07.2024

addition, such networks have a high cost and it is still unclear whether the BRICS consortium will be able to implement a network of at least four 1 m telescopes soon enough.

Short-range detection mode requires a large network of small-aperture wide-angle telescopes. These instruments are cheaper than 1 m telescopes and the network can be partially implemented even on national basis. Telescopes should be more or less evenly distributed around the globe.

In [10] a dedicated network of robotic telescopes to detect 10 m asteroids coming to the near-Earth space was proposed. The main features of the project INF (INASAN NEO Finder) are: short cadence time (1 h) of all-sky survey, a moderate limiting magnitude (19^m) without filters and a possibility of carrying out the additional scientific program. View of the one telescope of the INF system and main technical characteristics are shown in Fig. 4, left panel. The double-tube INF prototype is installed in the dome at Kislovodsk station of INASAN (see Fig. 4, right panel).

In Table 2 characteristics of other similar project (SuperWASP, ADAM-WFS¹¹, and GWAC) are presented. We believe that the main advantage of the INF is a better combination of the field of view, sensitivity, and the spatial resolution (pixel scale).

Table 2: INF comparison with other similar projects.

Parameter	INF	SuperWASP	ADAM-WFS	GWAC
Telescope aperture, mm	250	200	300	180
Pixel format	6k×6k	2k×2k	4k×4k	4k×4k
Field of view, deg ²	574	482	100	5000
Field of view of single tube, deg ²	72	60	25	164
Pixel scale, arcsec ⁻¹	5.2	13.7	4.36	11.2
All-sky survey	1 h @ 19^m	40 min @ 15^m	2 h @ 17.5^m	2 min @ 16^m

Besides NEOs detection, the INF has potential to work on other scientific programs such as gravitational wave events electromagnetic counterparts, variable stars, supernovae, gamma ray bursts and monitoring of space debris.

For fast repointing the INF multiaperture telescope will be installed in a “shell type” dome (see Fig. 5, left panel). The double-tube INF prototype is installed in the dome at Kislovodsk station of INASAN (Fig. 5, right panel).



Figure 5: Left: the INF multiaperture telescope concept: 8×VT-78d tubes on ASA DDM160 mount. Right: the double-tube INF prototype is installed in the dome at Kislovodsk station of INASAN.

To provide 24/7 operation and to detect NEOs coming from $2\pi+$ sr (night sky), several INF multiaperture telescopes are required to be installed in the northern and southern hemispheres at sites with low sky background. It is possible to put a filter change mechanism with one specific filter for each telescope. All telescopes can be aligned by a special mechanism to look at one eld in order to perform multicolor photometry or improve telescope

¹¹<https://fmph.uniba.sk/en/microsites/daa/division-of-astronomy-and-astrophysics/research/adam-wfs/>

sensitivity (20.4^m for 100 s exposure). For specific scientific tasks INF can be used for high time resolution photometry with a frame rate up to 44 Hz.

More that 20% of NEOs come into the near-Earth space from the day-time sky. Neither ground-based telescopes nor telescopes at LEO and GSO are capable of observing such day-time bodies. In [11] it is shown that the implementation of a system for the nearby detection of asteroids arriving from the day-time sky requires the use of a space-based system. The update concept of such system is described in paper by Shugrov&Shustov in this issue.

All of the above related to the hardware part of the telescope network of the project BITDN, but apparently the most difficult problem will be the organization of planning and real-time processing of a huge amount of data. Both observation planning and scheduling, and also analysis of observational data are still a major challenge for proposed BITDN network. Most promising is a fully robotic planning, scheduling and observation pipeline that extends the widely used open-source cross-platform software. This issue requires very serious attention.

The NEO problem is global in nature. This implies the necessity of international cooperation. The BRICS network is considered to work in close collaboration with Minor Planet Center¹², International Asteroid Warning Network¹³ and other international structures that work on the NEO problem.

References

1. D. Buckley, V. McBride, U. Barres De Almeida, B. Shustov, et al., *Anais da Academia Brasileira de Ciencias*, **93**, e20200917, 2021.
2. M. Granvik, A. Morbidelli, R. Jedicke, B. Bolin, et al., *Icarus*, **312**, 181, 2018.
3. D. Nesvorny, R. Deienno, W. F. Bottke, R. Jedicke, et al., in *Asteroids, Comets, Meteors Conference*, **2851**, 2123 (2023).
4. G. Marchiori, M. Tordi, L. Ghedin, J. Martinez, C. Manfrin, C. Battistel, R. Messing, and E. Doelling, in H. K. Marshall, J. Spyromilio, and T. Usuda, eds., *Ground-based and Airborne Telescopes IX*, **12182**, 121824K (2022).
5. Ž. Ivezić, S. M. Kahn, J. A. Tyson, B. Abel, et al., *Astrophys. J.*, **873**, 111, 2019.
6. A. K. Mainzer, J. R. Masiero, P. A. Abell, J. M. Bauer, et al., *Planetary Science Journal*, **4**, 224, 2023.
7. B. M. Shustov, S. A. Naroenkov, V. V. Emel'yanenko, and A. S. Shugarov, *Solar System Research*, **47**, 288, 2013.
8. T. Hoffmann, M. Gehlen, T. Plaggenborg, G. Drolshagen, et al., *Frontiers in Astronomy and Space Sciences*, **9**, 895732, 2022.
9. J. Liu, R. Soria, X.-F. Wu, H. Wu, and Z. Shang, *Anais da Academia Brasileira de Ciencias*, **93**, 20200628, 2021.
10. A. Shugarov, M. Nalivkin, S. Naroenkov, and I. Savanov, *Contributions of the Astronomical Observatory Skalnaté Pleso*, **49**, 293, 2019.
11. B. M. Shustov, A. S. Shugarov, S. A. Naroenkov, and M. E. Prokhorov, *Astronomy Reports*, **59**, 983, 2015.

¹²<https://minorplanetcenter.net/>

¹³<https://iawn.net/>

Содержание

<i>Джафарпур М.Х. и др.</i> Восстановление коронального магнитного поля при помощи ограниченной оптимизации по данным SDO/HMI	35
<i>Зинченко И.И.</i> Аккреционные вспышки в массивных молодых звездных объектах	40
<i>Усанин В.С.</i> К вопросу о существовании кометного семейства Урана	44
<i>Кузнецов Э.Д., Галиуллин М.И., Гламазда Д.В., Вибе Ю.З.</i> Динамические и физические параметры астероидов, сближающихся с Землей, по данным наблюдений на телескопе СБГ	47
<i>Сергиенко М.В., Нefeldьев Ю.А., Андреев А.О.</i> Анализ динамических параметров метеорного комплекса Канкрид и его дрейфового движения	52
<i>Коротышкин Д.В., Шерстюков О.Н., Валиуллин Ф.С.</i> Перспективы развития метеорных радиолокационных наблюдений в Казанском федеральном университете	55
<i>Шугаров А.С., Шустов Б.М.</i> О синергии наземных и космических телескопов при обнаружении ОСЗ декаметрового класса в околоземном космическом пространстве	65
<i>Шустов Б.М.</i> Малые тела Солнечной системы: научные и практические вопросы проекта BITDN	73

Contents

<i>Jafarpour M.H. et al.</i> Reconstruction of coronal magnetic field by constraint optimization using the SDO/HMI data	35
<i>Zinchenko I.I.</i> Accretion outbursts in massive young stellar objects	40
<i>Usanin V.S.</i> Concerning the existence of the Uranus comet family	44
<i>Kuznetsov E.D., Galiullin M.I., Glamazda D.V., Wiebe Yu.S.</i> Dynamic and physical parameters of near-Earth asteroids from SBG telescope observations	47
<i>Sergienko M.V., Nefedev Y.A., Andreev A.O.</i> Analysis of the dynamic parameters of the Cancrids meteor shower and its drift motion	52
<i>Korotyshkin D.V., Sherstyukov O.N., Valiullin F.S.</i> Prospects for development of meteor radar observations at Kazan Federal University	55
<i>Shugarov A.S., Shustov B.M.</i> On the synergy of ground-based and space telescopes in the discovery of decameter class NEOs in the near-Earth space	65
<i>Shustov B.M.</i> Small bodies of the Solar system: scientific and practical issues for the BITDN	73